# Functional effects of distinct innervation styles of pyramidal cells by fast spiking cortical interneurons

Yoshiyuki Kubota, Satoru Kondo, Masaki Nomura, Sayuri Hatada, Noboru Yamaguchi, Alsayed A Mohamed, Fuyuki Karube, Joachim Lübke, Yasuo Kawaguchi

DOI: http://dx.doi.org/10.7554/eLife.07919

Cite as: eLife 2015;10.7554/eLife.07919

Received: 3 April 2015
Accepted: 4 July 2015
Published: 4 July 2015

# Title: Functional effects of distinct innervation styles of pyramidal cells by fast spiking cortical interneurons

**Authors:** *Yoshiyuki Kubota[1,2,3], Satoru Kondo[3,4], #Masaki Nomura[3,5], Sayuri Hatada[1], Noboru Yamaguchi[1], Alsayed A. Mohamed[1,6], Fuyuki Karube[1,3,7], Joachim Lübke[8,9,10], Yasuo Kawaguchi[1,2,3]

**Affiliations:**

[1] Division of Cerebral Circuitry, National Institute for Physiological Sciences, Okazaki, Aichi 444-8787, Japan.
[2] Department of Physiological Sciences, The Graduate University for Advanced Studies (SOKENDAI), Okazaki, Aichi 444-8585, Japan.
[3] Japan Science and Technology Agency, Core Research for Evolutional Science and Technology, Tokyo 102-0075, Japan.
[4] Department of Physiology, Kyushu University, Fukuoka 812-8582, Japan.
[5] Department of Mathematics, Kyoto University, Sakyo-ku, Kyoto, Kyoto 606-8502, Japan.
[6] Department of Anatomy & Embryology, South Valley University, Qena 83523, Egypt
[7] Laboratory of Neural Circuitry, Gradate School of Brain Science, Doshisha University, Kyotanabe, Kyoto 610-0394, Japan
[8] Institute for Neuroscience and Medicine INM-2, Research Centre Jülich, 52425 Jülich, Germany.
[9] Department of Psychiatry, Psychotherapy and Psychosomatic, Medical Faculty, RWTH/University Hospital Aachen, 52074 Aachen, Germany.
[10] JARA Translational Brain Medicine, Germany.
# present address: Center for iPS Cell Research and Application (CiRA), Kyoto University, Kyoto 606-8507, Japan

Contact information: yoshiy@nips.ac.jp

*Corresponding Author: Yoshiyuki Kubota, Ph.D.
Division of Cerebral Circuitry,
National Institute for Physiological Sciences
5-1 Myodaiji-Higashiyama
Okazaki, Aichi 444-8787, Japan
Phone: +81-564-59-5282, e-mail: yoshiy@nips.ac.jp

4,696 words main text, 10 figures, 10 secondary figures, 6 Tables, 48 pages

## Abstract

Inhibitory interneurons target precise membrane regions on pyramidal cells, but differences in their functional effects on somata, dendrites and spines remain unclear. We analyzed inhibitory synaptic events induced by cortical, fast-spiking (FS) basket cells which innervate dendritic shafts and spines as well as pyramidal cell somata. Serial electron micrographs (EMgs) reconstruction showed that somatic synapses were larger than dendritic contacts. Simulations with precise anatomical and physiological data reveal functional differences between different innervation styles. FS cell soma-targeting synapses initiate a strong, global inhibition, those on shafts inhibit more restricted dendritic zones, while synapses on spines may mediate a strictly local veto. Thus, FS cell synapses of different sizes and sites provide functionally diverse forms of pyramidal cell inhibition.

## Introduction

Microcircuits of cerebral cortex are composed of excitatory pyramidal cells and different types of GABAergic interneurons. Inhibitory circuits regulate cortical activity(Kubota 2014; Kubota, Shigematsu, et al. 2011; Lee et al. 2012), development and plasticity(Donato, Rompani, and Caroni 2013; Hensch 2005). Perturbed inhibitory function is associated with pathologies including epilepsy, autism and schizophrenia(Gonzalez-Burgos, Hashimoto, and Lewis 2010; Rubenstein and Merzenich 2003). However, mechanisms controlling inhibitory synaptic actions are incompletely understood. For instance, inhibitory synapses target multiple membrane domains of pyramidal cells: soma, axon initial segment, dendritic shafts and spines(Jiang et al. 2013; Kawaguchi and Kubota 1998; Kisvarday et al. 1985; Kubota et al. 2007; Szabadics et al. 2006). Contacts at these different sites produce inhibitory postsynaptic potentials (IPSP) with different properties(Miles et al. 1996; Xue, Atallah, and Scanziani 2014).

Recent data suggests IPSCs generated by FS basket cells may be matched to the level of synaptic excitation in cortical pyramidal cells(Xue, Atallah, and Scanziani 2014), and differ with target cell subtypes(Lee et al. 2014). Unitary inhibitory postsynaptic currents (uIPSCs) are significantly smaller in neurons of Disc1 mice, a genetic model of depression, and may underly reduced low-gamma oscillations in the frontal cortex (Sauer, Struber, and Bartos 2015). GABA receptors on spine heads are thought to control local synaptic excitation(Chiu et al. 2013). However the structural basis for these effects remains unclear. Modeling studies assume that somatic, dendritic shaft and spine inhibition is mediated by pre-synaptic elements of identical size and strength(Gidon and Segev 2012). In contrast, excitatory synaptic terminals vary in size and their strength is correlated with terminal size(Holderith et al. 2012). We therefore examined this point for cortical inhibition by correlating structural and functional properties of synapses of

FS basket cells on layer V (L5) pyramidal cells of rat frontal cortex. Physiological and anatomical data from paired records let us simulate the dendro-somatic conduction of the effects of inhibitory synapses made on different membrane sites on pyramidal cells. We show that synapses made by FS basket cells on the soma and on dendritic shafts and spines have dramatically different functional effects.

## Results

*Double recording*

Crossed-corticostriatal (CCS) 'slender untufted' pyramidal cells(Larkman and Mason 1990) are a discrete neuronal population in L5. We investigated connections between FS basket cells and CCS pyramidal cells, identified by injecting a fluorescent retrograde tracer into the contralateral striatum (**Figure 1-figure supplement 1**). IPSCs were evoked in postsynaptic CCS pyramidal cell soma by single action potentials in FS basket cells (**Figure. 1-figure supplement 2**). With pyramidal cell membrane potential maintained at -65 mV, IPSCs reversed on average at -52.5 mV (**Figure. 1-figure supplement 2C**), providing a mean driving force of 12.5 mV. After recording and biocytin-filling, axonal and dendritic morphology and the number and distribution of possible synaptic contacts from each coupled pair were analyzed (n=10) using *Neurolucida* software (**Figure. 1B-E, G-I, Figure. 2A-D, F-I**). Paired recordings were made from neighboring cells (**Table 1**, inter-somatic distance: 44.5 ± 23.7 μm, 20.6 – 66.6 μm). There was typically a large overlap of the basal dendrites of postsynaptic pyramidal cells and the axonal arbor of presynaptic FS basket cells (**Figure. 1B, G, Figure. 2B, G, Figure. 2-figure supplement 1**). In three cell pairs, FS basket cell axons made putative synaptic contacts on the soma and dendrites of a postsynaptic CCS pyramidal cell (**Figure. 1J, upper three lines**). In seven pairs, synaptic contacts were located exclusively on dendrites at varying distances from the soma (**Figure. 1J, lower 7 lines**). The number of putative synaptic contacts was 5-14 (8.2 ± 4.8, 10 pairs). Most LM contacts were made where FS basket cell axons crossed basal pyramidal cell dendrites (**Figure. 1D, E, H, I, Figure. 2D, I, Figure. 3B, Figure. 5F, J)**(Marlin and Carter 2014). The distance from the soma of dendritic contacts was 5.8-208.4 μm with a mean value of 82.5 ± 50.0 μm. Peak IPSC amplitude was larger in pairs with putative somatic contacts than

when contacts were exclusively dendritic (**Figure. 1J**). Transmission never failed for pairs with somatic contacts but failures occurred with dendritic contacts (**Table. 1**). Mean IPSC amplitude, from pairs with only dendritic contacts, was reduced at increasing distances from the soma to the nearest contact (**Figure. 1J**). IPSCs were not detected in two pairs, where light microscopy (LM) suggested 7 and 9 contacts were made at distances greater than 33 μm from the soma (**Figure. 1j, lower 2 lines**). In each case the pyramidal cell elicited large EPSC in the interneurons (**Table. 1**).

We found large differences in IPSC amplitude evoked by FS cells in L5 pyramidal cells (**Figure. 1A, F, J, Figure. 2E, J**). Large IPSCs were found in two pairs with somatic synaptic contacts. The size of IPSCs in the other pair with somatic/dendritic contacts was smaller (**Figure. 1J).** Higher numbers of putative somatic terminals were correlated with larger synaptic events (**Figure. 2C, D, H, I**). Thus the number of intersections of the presynaptic FS cell axon fibers within 18 μm from somatic center were larger in the pair CS55 with an IPSC of amplitude -91.3 pA than the pair CS56 where IPSC amplitude was -17.3 pA (**Figure. 2-figure supplement 2**).

*Synapses identified by 3D reconstructions from serial EMgs*

The number of synaptic terminals was verified and their size measured using electron microscopy (EM). Junctional size governs transmitter release probability(Holderith et al. 2012) and docking sites(Pulido et al. 2015), which with the number of postsynaptic receptors(Nusser, Cull-Candy, and Farrant 1997; Tanaka et al. 2005)determines synaptic current amplitude. All synaptic contacts (**Figure. 2D, I**) were completely reconstructed from serial EMgs (**Figure. 3, Figure. 3-figure supplement 1**) for measurement of synaptic junction and dendritic cross sectional areas. Similar data from sixty one dendritic segments (mean length 16.8 ± 6.8 μm) of the CS56 postsynaptic pyramidal cell and the entire soma of the pyramidal cell (**Figure. 4**) was

also used in neuron simulations(Kubota, Karube, et al. 2011).

EM analysis let us verify possible synaptic contacts from LM. For the pair CS56, 3 of 7 possible contacts were verified by EM, but no synaptic contact was made at 4 other potential sites (**Figure. 4**). One putative LM contact was resolved as three distinct *en passant* boutons (S1-S3 in **Figure. 5A-E**) and another somatic contact was detected only by EM (S4, **Figure. 5-figure supplement 1**). Three of these 6 verified contacts terminated on spine heads (Sp2, Sp3 in **Figure. 6A, C** and Sp1, **Figure. 5F-I, Figure. 6A, C**) and one with a thin dendrite (D1 in **Figure. 5F, G, I, Figure. 6A, C;** not in LM). The junctional area of synapses made by single interneurons varied strikingly with the post-synaptic site that is innervated. For somatic synapses junctional area was 0.194 – 0.350 $\mu m^2$, it was 0.102 $\mu m^2$ for synapses with dendritic shafts and 0.042 - 0.056 $\mu m^2$ for synapses onto spine heads (**Figure. 6F, Table 2**). Axonal bouton volume was linearly correlated with synaptic junction area (**Figure. 6-figure supplement 1A**).

Fourteen potential contacts, 3 at somatic and 11 at dendritic sites, were identified by LM for the pair CS55 (**Figure. 2I**). Complete EM reconstruction of the post-synaptic soma let us explore sites obscured in LM where axon crossed the soma (**Figure. 5J-N, Figure. 5-figure supplement 2)** and revealed 13 synaptic contacts (S1-S13, **Figure. 5M, N, Figure. 6B, E, G**). Eight terminals made onto dendrites and spine heads less than 33 μm away from the soma presumably contributed to the somatic IPSC (**Figure. 5J, Figure. 6B, D, E, G**). Three dendritic shaft synapses (D5-D7), were located further than 33 μm from soma. Five potential LM contacts were discounted from EM data (**Figure. 5-figure supplement 3**), and 4 synapses were only evident in EM. 3D EM reconstructions of all synapses (CS55 and CS56) showed that synaptic area was larger for somatic than dendritic contacts (**Figure. 6G**, **Table 3**) and decreased continuously with distance from the soma.

Numbers of synaptic contacts were defined for two further neuron pairs, CS44 and CS23, by serial EMgs (**Figure. 1J)**. In the CS44 cell pair the closest confirmed synaptic contact was 32 μm distant from the soma, consistent with the inverse relation between synapse distance from the soma and the peak IPSC amplitude (**Figure. 6E)**. In pair CS23, EM verified five dendritic synaptic contacts with the nearest contact site 53 μm from the soma. Physiological analysis revealed the connection was nearly silent (**Figure. 6E)**. IPSCs induced by single FS interneurons at dendritic shaft synapses at 32 μm from soma (CS44) were detected with a somatic electrode, but with our recording configuration, IPSCs generated by terminals at 47 μm (CS10) and 53 μm (CS23) from the soma were not detected.

Three types of FS basket cell innervation can then be distinguished. Multiple synapses made with the soma or proximal dendrites of L5 CCS pyramidal cell produce large IPSCs, weaker somatic and proximal dendritic innervation produce intermediate IPSCs, while IPSCs are small or absent when synapses terminate exclusively on dendrites. From all paired records, 28.4 ± 7.6% (17.2 - 43.1%) of FS interneuron terminals contacted cell somata (**Figure. 5, Figure. 5-figure supplement 3A, Table. 4),** consistent with previous data(Karube, Kubota, and Kawaguchi 2004). We note that an FS cell that innervates only dendrites of one L5 pyramidal cell, may contact somatic sites of other postsynaptic neurons (**Figure. 7)**.

*Simulation analysis of IPSC conduction*

Excitatory synaptic currents are correlated with synaptic size(Holderith et al. 2012). At larger synaptic junctions, Ca entry into presynaptic terminals is greater, transmitter release probability is increased(Holderith et al. 2012) and the number of postsynaptic receptors is larger(Nusser, Cull-Candy, and Farrant 1997). We tested this relation for inhibitory transmission by comparing

summed synaptic junction area with maximal IPSC amplitude for pairs CS56 and CS55. Maximal IPSCs (**Table 5**) were assumed to occur when all somatic and proximal dendritic terminals (< 33 μm) (**Figure. 5A-E**) released transmitter. The unit electrical charge was calculated as the maximum charge divided by the summed junction area of S1-S4: 326.1 fC/0.95 $\mu m^2$, or, 343.3 $fC.\mu m^{-2}$ for pair CS56, and S1-S13, D1-D4, Sp1-Sp4: 1057.8 fC/3.011 $\mu m^2$, or 351.3 $fC.\mu m^{-2}$ for pair CS55 (**Table 6**). This parameter was similar for the two connections, suggesting that currents are well correlated with synaptic junction area. Thus at these inhibitory synapses, conductance can be calculated from junctional area based on the unit IPSC electric charge using morphologically realistic CS56 postsynaptic pyramidal model cell based on our measurement of the cell dimensions (see method, **Table 2**).

Inhibitory synaptic connections made by FS basket cell axons terminate on the soma, dendritic shafts or spines of L5 CCS pyramidal cells(Kubota et al. 2007). We asked how these differences in synaptic site and junctional size affect function in simulations based on our measurements of synaptic currents and dimensions. IPSC propagation was examined on an electrotonic simulation of the pyramidal cell from pair CS56. Injecting a 0.11 nS current on the spine head of Sp1 (**Table 2**) resulted in a strong 0.78 mV hyperpolarization of the spine, but only 0.12 mV was transmitted to the basal dendrite and 0.07 mV to the soma (**Figure. 8A, C, K**). The peak synaptic current was 1.27 pA at the spine head, and 0.81 pA at the soma (**Figure. 8B**). At noise levels of ~10 pA (**Figure. 1-figure supplement 2B**), a spine-head IPSC would not be detected at the soma. The spine neck effectively isolated the spine head from the dendritic shaft (neck length, 0.5 μm; diameter, 0.07 μm; volume, 0.043 $\mu m^3$; resistance, 500 MΩ(Harnett et al. 2012)). Thus spine inhibition did not change nearby dendritic shaft or somatic potential (Araya et al. 2006). In contrast, injecting a 0.21 nS synaptic current on the dendritic shaft (D1) (**Table 2**) caused a

hyperpolarization of 0.23 mV on the shaft and 0.13 mV at the soma (**Figure. 8D, F, K**). The spine head Sp1 was hyperpolarized without attenuation(Harnett et al. 2012), while the D1 synapse reached only 30% of the Sp1 synapse peak membrane potential. The peak synaptic current was 2.45 pA at the spine head, and 1.55 pA at the soma (**Figure. 8E**). Injecting a synaptic waveform of 0.71 nS at the soma (S1) (**Table 2**) hyperpolarized that site by 0.48 mV (**Figure. 8G, H**) resulting in an IPSC of 8.29 pA (**Figure. 8H**), in the range of background noise. Simultaneous activation of somatic contacts S1-S4 resulted in a hyperpolarization of 1.33 mV, corresponding to a somatic current of 22.67 pA, (**Figure. 8I, J**) similar to IPSP amplitudes from paired records of FS basket cells to hippocampal pyramidal cells (0.5–3 mV)(Buhl, Halasy, and Somogyi 1994) and our own data (**Figure. 2e, Table 5)**. Thus for a similar driving force, proximal inhibitory synapses produce larger somatic hyperpolarizations than distal ones (**Figure. 8K)**.

Spines innervated by inhibitory synapses are typically excited by thalamic inputs(Kubota et al. 2007). We modeled the Sp1 spine to ask how spine-head IPSCs affect these excitatory thalamic signals(Gulledge, Carnevale, and Stuart 2012). Excitatory synaptic events (0.2 nS) were greatly reduced by a coincident spine-head IPSC (**Figure. 8L)**. Excitation of the spine-head site depolarized the pyramidal cell soma by 0.12 mV. Simulated release from four somatic inhibitory synaptic sites hyperpolarized the soma by 1.33 mV. Thus inhibition from clustered somatic synapses of one FS basket cell effectively suppressed dendro-somatic conduction of inputs from ~11 excitatory spine synapses. If release probability depends on terminal size(Holderith et al. 2012), then GABA may be infrequently liberated from smaller inhibitory terminals made by FS basket cells at dendritic sites. Since inhibitory synapses from a single cell usually contact different, distant dendrites, resulting hyperpolarizations may sum poorly (**Figure. 9**). Even so,

summation of integrated dendritic signals during inhibitory cell firing at frequencies of 40-50 Hz(Isomura et al. 2009) together with GABAergic shunting effects(Gidon and Segev 2012) may permit FS cell synapses to suppress excitatory inputs on innervated dendritic branches(Cossart et al. 2001). Diffusely situated inhibitory terminals on dendritic shafts can therefore effectively control afferent excitatory signals.

Variation in release from single synaptic boutons contributes to event-by-event fluctuations in post-synaptic currents(Sasaki, Matsuki, and Ikegaya 2012). IPSC amplitude varied substantially between trials in all dual recordings (**Figure. 8N, O, Table 5**). Monte Carlo simulations were made on the model of pair CS56 to ask whether this variability might result from probabilistic IPSC generation at somatic terminals, S1-S4 (**Figure. 8P)**. Mean IPSC charge transfer was 193.1 fC ± 56.2 (89.9 – 326.1 fC, n=60 traces; **Table 5**), with putative electric charge at somatic synapses calculated by multiplying junctional size by unit electrical charge, S1-S4 to give 120.1, 59.7, 66.6 and 79.6 fC respectively (**Table 2**). Release probability (0.59) was obtained by dividing the average electrical charge, 193.1 fC, by the maximum charge, 326.1 fC (**Table 5**). Somatic synapses were activated randomly with release probabilities correlated with junctional area (S1: 0.8. S2: 0.4, S3: 0.45, S4: 0.55) (**Figure. 8-figure supplement 1**) (Holderith et al. 2012). IPSC charge distributions from paired records and simulations were statistically similar (P = 0.41 Kolmogorov-Smirnov, **Figure. 8N, P)**, suggesting that IPSC amplitude variations result from an independent, stochastic activation of individual somatic and proximal synapses(Sasaki, Matsuki, and Ikegaya 2012).

*General principle of cortical inhibitory connections*

We suggest that FS cell inhibitory synaptic strength is progressively reduced from terminals

242 contacting the soma to dendritic shafts and then spines of target pyramidal cells. We asked
243 whether this represents a general principle for cortical inhibitory connections by comparing
244 synapses made by different classes of cortical interneurons stained using whole cell recording
245 method (**Figure. 10A**)(Kubota et al. 2007). 3D reconstruction of serial EMgs let us calculate
246 synaptic junction area and the cross sectional area of postsynaptic dendrite or spine volume, for
247 305 synapses made by 9 different types of interneuron. The junctional area of somatic inhibitory
248 synapses was 0.40 ± 0.15 $\mu m^2$ (n=23), for dendritic shaft synapses it was 0.19 ± 0.12 $\mu m^2$
249 (n=195) and for synapses terminating on spines it was 0.09 ± 0.05 $\mu m^2$ (n=87). Synaptic
250 junctional area was therefore correlated with the size of the target structure (**Figure. 10B-L**) with
251 the possible exception of Martinotti cell terminals (**Figure. 10J**) that contact distal pyramidal cell
252 dendrites(Silberberg and Markram 2007). Linear relations between synapse junction and post-
253 synaptic target size (**Figure. 10B-L**) may provide an effective impedance matching (Kubota and
254 Kawaguchi 2000) and thus control the inhibitory efficacy at different sites. Thus the variation in
255 effects of FS basket cell synapses targeting different membrane regions on L5 pyramidal cells
256 may reflects a general principle for inhibitory cortical circuits.
257
258 **Discussion**
259 These data show that FS basket cells mediate either a global somatic inhibition of variable
260 strength, a local dendritic shaft inhibition or act as a local veto at single spines. These distinct
261 effects depend on differences in junctional size. Local spine or shaft potential changes are small
262 and locally restricted. In contrast, somatic inhibitory currents are large, and summation of events
263 from several somatic terminals produces a global control of pyramidal cell excitation. Somatic
264 junctions have large areas, suggesting high release probability(Holderith et al. 2012) and

typically contact multiple sites(Buhl, Halasy, and Somogyi 1994). This enhances the likelihood of simultaneous release as FS cells fire repetitively at 30–50 Hz during motor behaviors in vivo(Isomura et al. 2009). Some FS basket cell connections with pyramidal cells involved exclusively dendritic sites while others consisted of both peri-somatic and proximal dendritic contacts. Spines receiving inhibitory synapses are typically large(Kubota et al. 2007) and their thalamic excitatory inputs presumably express both NMDA and AMPA receptors(Kubota et al. 2007; Matsuzaki et al. 2004). Inhibitory synapses may then efficiently veto these thalamic inputs before activation of NMDA receptors(Gulledge, Carnevale, and Stuart 2012) so reducing the probability of pyramidal cell firing.

In paired records IPSCs were detected only for terminals that contacted proximal pyramidal cell dendrites. However, IPSCs initiated on distal dendrites have been recorded at the soma in some studies(Jiang et al. 2013; Silberberg and Markram 2007). Possibly differences in experimental paradigm are responsible. In this work post-synaptic potentials were more hyperpolarized (-65 mV rather than -55/-57 mV) and $Cl^-$ in the recording pipette was higher (19 rather than 10 mM) than in other studies. Both differences would encourage somatic propagation IPSPs initiated at distant dendritic sites. In our somatic records we did not detect IPSPs generated at synapses more distant than ~40 μm. Possibly, the $Cl^-$ reversal was similar to the holding potential resulting in a small or null driving force at these sites. Indeed unperturbed $Cl^-$ reversal potentials may be 10-25 mV more hyperpolarized than in invasive whole-cell recordings(Bevan et al. 2000; Verheugen, Fricker, and Miles 1999). Further work is needed to define unperturbed $Cl^-$ reversal potentials in the dendrites and soma of L5 pyramidal cells.

Distinct numbers and sites of synaptic contacts made by FS interneurons with pyramidal cells may be regulated by network function(Yoshimura, Dantzker, and Callaway 2005) and activity

during different states(Klausberger and Somogyi 2008; Puig, Ushimaru, and Kawaguchi 2008). The strength of inhibition mediated by hippocampal FS basket cells varies with different target pyramidal cells. Synaptic strength is greater at connections with CA1 pyramidal cells of deep rather than superficial layers of stratum pyramidale(Lee et al. 2014) and it is genetically coded(Donato et al. 2015). The innervation patterns of cortical basket cells appear to be regulated by experience, environment or fear conditioning(Donato, Rompani, and Caroni 2013), according to network properties(Lee et al. 2014; Yoshimura, Dantzker, and Callaway 2005) and the activity in specific target cells(Xue, Atallah, and Scanziani 2014), and activity level of them may be regulated by learning as well as genetics(Donato et al. 2015). In contrast, the efficacy of synapses made by Martinotti cells seems to be independent of target pyramidal cell activity(Xue, Atallah, and Scanziani 2014). Thus different cortical interneurons respond in distinct ways to neuronal network state.

The size, and thus efficacy, of synaptic terminals made by FS interneurons with the soma, dendritic shafts and spines of target pyramidal cells were measured from 3D EM reconstructions. Other GABAergic interneurons make domain-specific contacts(Jiang et al. 2013; Kawaguchi and Kubota 1998; Kubota 2014; Marlin and Carter 2014). Paired recordings from other cortical interneurons and pyramidal cells followed by complete reconstruction of terminals will be needed to establish rules relating terminal size to efficacy. Nevertheless a somato-dendritic gradient of inhibitory terminal size may be a general principle. Our data suggests that relations between post-synaptic site, terminal properties including junctional area, and GABA release patterns may be maintained for other types of cortical interneuron.

Inhibitory synapses terminating on spines form 25–50% of GABAergic contacts with cortical pyramidal cell(Kubota et al. 2007; Chen et al. 2012) and so form a major part of inhibitory

311 microcircuits. Spines contacted by an inhibitory synapse are typically co-innervated by an
312 excitatory thalamic input(Kubota et al. 2007). Our simulations show single inhibitory synapses
313 can effectively veto synaptic excitation and intercept NMDA current(Chiu et al. 2013; Gulledge,
314 Carnevale, and Stuart 2012; Harnett et al. 2012) at the spine head. They could then prevent
315 summation of thalamic excitatory inputs arriving within about 20 ms(Marlin and Carter 2014), as
316 pyramidal cell and FS basket cells are co-activated by thalamo-cortical afferents(Kimura et al.
317 2010). The FS basket cell acts as a feed forward inhibition of thalamic input.

318 Excitatory synapses innervating cortical pyramidal cell spines can be modulated by visual
319 experience(Chen et al. 2012) or by somatosensory stimulation(Knott et al. 2002). The veto by
320 inhibitory synapses terminating on spines may be especially important for such plastic
321 changes(Chen et al. 2012). Pyramidal cell dendritic spines are tuned to distinct modalities and
322 spines with similar preferences cluster together on the same dendritic branch(Chen et al. 2013).
323 Inhibitory synapses on dendritic shafts may then inhibit tuned/non-tuned excitatory inputs on the
324 same but not different dendritic branches and so efficiently and specifically adjust pyramidal cell
325 activity(Liu 2004; Marlin and Carter 2014). Our data shows dendritic IPSCs may exert strictly
326 local effects. $Cl^-$ reversal potential at distal dendrite/spine synapses may normally be close to the
327 local resting membrane potential. However this small driving force would be increased by
328 depolarization due to dendritic EPSPs. IPSPs will then reduce EPSP amplitude at the soma even
329 if they do not propagate somatically. FS cells can thus control excitation of L5 pyramidal cells
330 by a specific, local veto of co-innervated spines, by reducing dendritic propagation of summed
331 EPSPs as well as by a strong, global peri-somatic inhibition.

332 We have estimated a peak amplitude of 5.7 ± 3.1 pA for EPSCs generated at single synaptic
333 contacts with CCS pyramidal cell proximal dendrites(Morishima et al. 2011). Here we found a

peak IPSC amplitude of 2.4 pA at dendritic shaft synapses. Our simulations suggest that summation of single excitatory and inhibitory synaptic currents may reduce dendritic excitation and suppress calcium entry via NMDA receptors(Larkum et al. 2009). $GABA_A$ receptor activation will also reduce EPSP amplitude by shunting(Gidon and Segev 2012; Hao et al. 2009). Thus, activation of a single dendritic inhibitory synapse should effectively suppress EPSCs at nearby excitatory synapses. This distal dendritic inhibition is functionally strong(Gidon and Segev 2012; Cossart et al. 2001). Inhibitory synapses on dendrites and spines act to reduce neuronal excitability by blocking local EPSCs and so decrease the amplitude of summed EPSPs. The synchronization of FS basket cell activity via gap junctions(Gibson, Beierlein, and Connors 1999) will further counter the summation of afferent EPSPs.

It is generally accepted that synaptic contacts detected by LM must be confirmed with EM. We verified 14 synapses of 25 putative dendritic contacts with LM (56%) in this study and 78% in our previous study(Karube, Kubota, and Kawaguchi 2004). In addition, we newly found 6 dendritic/spine synapses with EM (30%; 6/20). Care must also be taken with somatic inhibitory terminals which are much smaller than the soma, so that terminals behind or in front of a soma may be impossible to resolve in LM. Indeed, we identified 14 somatic synapses with EM for CS55 and 4 somatic synapses with EM for CS56, although our estimation of the contacts with LM was three for the CS55 and one for the CS56 pair. Our data shows the importance of EM data for quantitative measurements on the number and size of synaptic junctions.

Passive cable properties and voltage-dependent resting conductances affect IPSP amplitude. Since postsynaptic target size is related to input resistance and synaptic junction area to the number of post-synaptic receptors(Nusser, Cull-Candy, and Farrant 1997), alterations in synaptic dimensions may govern the size of GABAergic currents. The dependence of synaptic terminal

areas on postsynaptic dendritic cross sectional areas would tend to maintain a constant ratio of synaptic conductance to post-synaptic input resistance. Thus, presynaptic interneuron actions are efficiently regulated to provide an appropriate hyperpolarization of their post-synaptic target(Kubota and Kawaguchi 2000).

EPSC amplitude is correlated with synaptic junction area, release probability, calcium entry and receptor number(Holderith et al. 2012). At inhibitory synapses, currents are also correlated with release probability, docking site number and receptor number(Nusser, Cull-Candy, and Farrant 1997; Pulido et al. 2015). Synaptic junctional area should then govern IPSC amplitudes. Surprisingly unit IPSCs from records in this work were quite similar, suggesting that the inhibitory synaptic current is well correlated with synaptic junction area. Larger synapses may generate larger IPSCs, due to multiple release sites or higher numbers of post-synaptic receptors. The presence of multiple release sites at some synaptic junctions has been shown by anatomy(Holderith et al. 2012; Nakamura et al. 2015) or estimated from neurophysiological data(Nakamura et al. 2015; Pulido et al. 2015). Clusters of the Cav2.1 Ca-channels in large synaptic junctions have been correlated with estimates of the number of vesicular docking sites. GABA release from multiple sites in a large synapse could saturate post-synaptic receptors and initiate large synaptic currents of similar amplitude, as at single-terminal synaptic connections made by molecular layer interneurons of the cerebellum. In contrast, the IPSCs examined here were mediated by multiple synaptic contacts of FS basket cells on L5 CCS pyramidal cells. IPSC amplitude fluctuations presumably reflected variations and failures in release from different terminals.

Axons of cortical non-pyramidal cells project to distinct laminar and columnar zones (Kubota 2014), enabling different subtypes of interneuron to form synapses with specific targets.

Projecting to a specified zone, an axon could make contacts nonspecifically with any available target neuron (Fino and Yuste 2011; Packer et al. 2013; Packer and Yuste 2011). Alternatively synaptic contacts may be established preferentially with specific neuronal subtypes or target domains, such as soma, axon or dendrites (Jiang et al. 2013). Target preference may depend on an activity dependent control of excitatory and inhibitory synaptic input size in order to maintain E/I balance (Xue, Atallah, and Scanziani 2014). Our data show FS basket cells may form synaptic contacts with the perisomatic region of post-synaptic pyramidal cells or with their proximal dendritic shafts and spines. Inhibitory synaptic junctional area was matched to the synaptic site – it was larger at somatic than dendritic sites and larger at synapses made with shafts than at those made with dendritic spines. Molecular cues to recognize a somatic or dendritic innervation site may include chemoattractive and cell adhesion molecules. Such mechanisms are involved in a segregation of dendritic spine inhibitory inputs and distinct sources of afferent excitation. Spines innervated by FS basket cell terminals also receive excitatory synapses from thalamus, but never recurrent cortical pyramidal cell inputs (Kubota et al. 2007). Both activity dependent chemoattractant factors (Yee et al. 1999) and cell adhesion molecules of the protocadherin family (Meguro et al. 2015; Yagi 2015) have been linked to this specificity. Functionally it would permit FS cell inhibitory synapses to mediate an efficient and selective veto on excitatory inputs from the thalamus.

A recent modeling paper(Gidon and Segev 2012) enhanced our understanding of dendritic inhibitory operations. It assumed that inhibitory synapses targeting pyramidal cell somata, dendritic shafts and dendritic spines possess a uniform size, and strength. Our data suggests the model could be refined to explore the effects of variation in synaptic size and strength from soma to dendrite spine. Quantitative 3-D EM reconstructions provide an exact basis to assign different

403 weights to inhibitory synapses that contact different sites. This inhibitory synaptic machinery
404 differs from that at excitatory synapses subject to both plasticity(Matsuzaki et al. 2004) and
405 scaling functions(Katz et al. 2009; Magee 2000). Defects in these microcircuits may contribute
406 to depression and other neuronal diseases (Sauer, Struber, and Bartos 2015). Our data thus
407 provide novel insights into biophysical design principles for inhibitory synaptic operations in
408 neural microcircuits.
409
410

411 **Materials and Methods**

412 **Retrograde labeling of CCS cells**

413 Retrograde labeling of CCS cells was performed as described previously (Morishima and
414 Kawaguchi 2006). Briefly, young Wistar rats (between postnatal 19–23 days old; Charles River,
415 Japan) were anesthetized with ketamine (40 mg/kg body weight) and xylazine (4 mg/kg body
416 weight). Rats were placed in a stereotaxic frame and the skull on the injection hemisphere was
417 partially removed and the cortex, hippocampus and fimbria caudal to the striatum were suctioned
418 to prevent the spilling of dye into the cortex during injection. Cholera toxin subunit B conjugated
419 with Alexa Fluor 555 (CTB-555; C34776, Invitrogen, NY, U.S.A.) was used as the retrograde
420 tracer (0.2 % dissolved in distilled water). Injection site was determined by using stereotaxic
421 coordinate (0.8 mm posterior to bregma, 2.5 mm lateral to the midline, depth 4 mm) and a glass
422 pipette (tip diameter is around 100 micron) filled with CTB-555 was inserted to the striatum
423 obliquely. Injection (80-100 nl) was performed using positive pressure from a pneumatic pico-
424 pump (PV-820, World Precision Instrument, Sarasota, FL, U.S.A.). After injection, the aspirated
425 brain space was filled with a gel sponge (Spongel, Astellas Pharma Inc., Tokyo, Japan) immersed
426 with saline and the skin was sutured. Rats recovered from surgery in the animal facility and were
427 used for electrophysiological experiments at 2-3 days after the injection.

428

429 **Slice preparation**

430 Rats were deeply anesthetized with isoflurane and were decapitated after the loss of all responses
431 to tactile stimuli, such as pinching legs. Slices of frontal cortex (300 μm thick) were cut in ice-
432 cold artificial cerebrospinal fluid ACSF with a vibratome (VT1000S, Leica, Germany) and kept
433 at room temperature in ACSF until recordings. The ACSF consisted of (in mM) 124 NaCl, 3 KCl,

2.4 $CaCl_2$, 1.2 $MgCl_2$, 26 $NaHCO_3$, 1 $NaH_2PO_4$, 20 glucose, 0.4 ascorbic acid, 2 pyruvic acid and 4 lactic acid and saturated with 95%$O_2$/5%$CO_2$.

**Paired recordings**

Slices were transferred to a recording chamber and perfused at 1-2 ml/min with ACSF (25 °C). Patch pipettes (3-5 MΩ) were pulled from borosilicate glass and filled with 20 µl of internal solution containing (in mM): 126 K-methylsulfate, 6 KCl, 2 $MgCl_2$, 0.2 EGTA, 4 ATP, 0.3 GTP, 10 phosphocreatine, 10 HEPES and 0.75% biocytin. The pH of the pipette solution was adjusted to 7.3 with KOH and the osmolarity was set to 295 mOsm. Potassium-methylsulfate as internal solution provided a physiological space clamp (Fleidervish and Libman 2008). Dual patch-clamp whole-cell recordings (EPC9/dual, HEKA, Germany) were made in the frontal cortex (medial agranular and anterior cingulate cortex) with the use of ×40 water-immersion objective (Axioskop FS, Carl Zeiss, Germany). Pipette resistance was 3-5 MΩ. Series resistance was typically 6-15 MΩ and was not compensated. If it exceeded 20 MΩ, data were discarded. Liquid junction potential was not corrected. The data were recorded at 10 kHz and filtered at 2 kHz. For paired whole-cell recordings, retrogradely labeled pyramidal neurons were selected under fluorescence and differential interference contrast microscope (DIC) (Stuart, Dodt, and Sakmann 1993). FS basket cells were identified in acute slices by their appearance under DIC microscopy. FS cells were recorded using the above internal solution, while pyramidal cells were recorded using an internal solution with the KCl concentration raised to 15mM and K-methylsulfate lowered to 117mM to depolarize the reversal potential of $Cl^-$ (-52.5mV). IPSCs were recorded as inward currents at -65 mV holding potential. APs were initiated in the presynaptic neuron by 1 ms depolarizing pulses of 300 pA. Presynaptic APs and postsynaptic currents were recorded

simultaneously.

**Electrophysiological data analysis (Figure. 1-figure supplement 2)**

Recorded presynaptic potentials and postsynaptic IPSCs were analyzed off-line with IGOR software (WaveMetrics, Lake Oswego, OR, U.S.A.). For the calculation of kinetic parameters of postsynaptic currents, traces with spontaneous synaptic currents on the rising or decay phase were omitted. The onset of the postsynaptic current was estimated by fitting the rising phase with a parabola and extrapolating back to the baseline. Postsynaptic current amplitude was measured as the difference between the peak current, measured from a 1.5 ms window centered at the peak, and the average baseline current, measured in a 4 ms window preceding the presynaptic AP. The decay time constant was obtained by fitting the decay phase of postsynaptic current with a double exponential equation. Since synaptic responses systematically run-down during the time course of some experiments, the amplitudes of postsynaptic currents were plotted against time and only stable periods were selected for further analysis. On average 100 traces (range 50-150) were analyzed for each experiment. Postsynaptic currents smaller than 2 times the noise level were discarded as failures, and the amplitudes of the remaining postsynaptic currents were analyzed. Cumulative histograms of postsynaptic current and noise were constructed and compared with a paired t-test and confirmed the separation between two （**Figure. 1-figure supplement 2B**）. To average postsynaptic currents, the peaks of the postsynaptic currents were aligned. The electric charge of IPSC was analyzed using AxoGraph (Molecular Devices, Sunnyvale, CA, U.S.A.). Values are reported as mean ± standard deviation.

**Visualization of recorded cells**

After electrophysiological records, slices were immersion-fixed (1.25 % glutaraldehyde, 4 % paraformaldehyde, 0.2% picric acid in 0.1 m phosphate buffer) and irradiated for 10 sec using a microwave, and kept at room temperature for 2 hours. Slices were then dehydrated and cryoprotected with sucrose containing 0.1 M phosphate buffer (15 % followed by 30 % of sucrose solution) and freeze-thawed in the liquid nitrogen. Slices were re-sliced at 50 μm thickness with the vibratome and reacted with avidin-biotin peroxidase complex solution (ABC kit, Vector Laboratory, Burlingame, CA, U.S.A.). Biocytin-filled cells were visualized with 3,3'-diaminobenzidine tetrahydrochloride (0.02 %), nickel ammonium sulfate (0.3 %), and $H_2O_2$ (0.004 %). Slices were further post-fixed in 1 % OsO4 with 7 % glucose and embedded in plastic (Epon 812 resin kit, TAAB, Aldermaston, U.K.) between silicone (Sigma coat, Sigma-Aldrich, U.S.A.) coated glass slide and cover slip.

**Morphological analysis**

Axons, dendrites, and somata of stained neurons were reconstructed using the *Neurolucida* software (MBF Bioscience, Williston, VT, U.S.A.) attached to a NIKON ECLIPSE microscope equipped with a 60x objective lens (N.A. 1.4, NIKON, Tokyo, Japan). Inter point interval of drawing axons and dendrites was less than 2 micron. No correction was made for tissue shrinkage, which should be about 90% (Karube, Kubota, and Kawaguchi 2004). Putative synaptic contacts were identified and their location was marked on the traces of axons and dendrites. The software *Neuroexplorer* was used for morphometrical and quantitative analyses of reconstructed cells, including total dendritic length and distances between somata and putative synaptic contacts.

**Focus stack image**

The dendritic segment or soma images of every 0.5 μm focus step in the same image field were captured using the *Neurolucida* software (MBF Bioscience, Williston, VT, U.S.A.) attached to a NIKON ECLIPSE microscope equipped with a 60x objective lens (N.A. 1.4, NIKON, Tokyo, Japan) and CCD camera (1392 x 1040 pixels). The focus stack image was obtained using 'auto-blend layers/stack images' function of Photoshop (Adobe, San Jose, U.S.A.), which combine the best focused area of the multiple focus step images, to give a greater depth of field (http://en.wikipedia.org/wiki/Focus_stacking).

**EM analysis**

After reconstruction with *Neurolucida*, stained neurons were serially sectioned at thickness 50 nm with an ultramicrotome (Reichert Ultracut S, Leica Microsystems, Germany). Ultrathin sections were mounted on Formvar-coated single-slot grids. EM images of labeled axon terminals and dendrites were captured with a CCD camera (XR-41, Advanced Microscopy Techniques, U.S.A.) in Hitachi H-7000, and HT-7700 EMs (Hitachi, Tokyo, Japan). Structures of interest were reconstructed and quantified from the serial EM images, with the 3D reconstruction software, Reconstruct (http://synapses.clm.utexas.edu/tools/index.stm) (Fiala 2005). The synaptic junctions were segmented at a typical cleft structure that was found between presynaptic vesicle aggregations and postsynaptic membrane density.

**Simulation analysis**

Simulations were made with NEURON (Hines and Carnevale 1997). The morphology of the model neuron was reconstructed from the EM imaging data. Pyramidal cell dendrites typically

possessed elliptical cross sections, but NEURON is limited to circular morphologies. We circumvented this problem by first modeling the pyramidal neuron with circular dendritic cross sections, preserving the cross sectional area from EM. Then, leak conductance and membrane capacitance densities in each section in the circular model were adjusted to be equivalent to those predicted from EM imaging data. Our pyramidal model incorporates passive leak channels only. The passive leak conductance and membrane capacity before adjustment were 0.0001 S/cm$^2$ and 1 μF/cm$^2$, respectively. The intracellular resistance for somata, basal and apical dendrites was 100 Ωcm, and for the spine head and spine neck 385Ωcm, respectively. The equilibrium potential of the leak current was set to -65mV. As above, the passive leak conductance and membrane capacitance density in each section in the NEURON model were modified in order to mimic the elliptical shape (for further details, refer to our previous paper (Kubota, Karube, et al. 2011)). The relationship between cross sectional area (S), circumference (L) and summed length of distal dendrites (R) we used here is (S)=0.00033258(R)+0.048097 and (L)=0.0012661(R)+1.3206.

The membrane potential was set to -65 mV (Morishima and Kawaguchi 2006), and the $GABA_A$ reversal potential to -77.5 mV (Gulledge and Stuart 2003) to fit our measurements of driving force. The electrical charge of each synaptic contact was calculated by multiplying the synapse junction area by the unit electrical charge; in turn individual synaptic conductance was calculated from the electric charge (**Table 2**). The synaptic current was adjusted to the average current of pair CS56 (**Figure. 2E, right panel**) with a double exponential fit. It was injected at sites where the presynaptic FS basket cell axon established synaptic contacts with the pyramidal cell.

A kinetic model was used for inhibitory synapses (Destexhe et al., 1994). Parameters were estimated by fitting the model to the unitary max IPSC data (**Figure. 2E left panel**). The estimated duration time, rise time constant, decay time constant and conductance are 2.3 ms,

549 0.45 ms, 14.17 ms and 1.92 nS, respectively. Individual synaptic conductance was estimated as
550 multiplying 1.92 nS (conductance of the unitary max IPSC) by the ratio of synaptic junctional
551 area of each synapse to the total area of the 4 somatic synaptic junctional area (0.950 $\mu m^2$). The
552 values of synaptic conductance corresponding to contact sites, S1, S2, S3, S4, D1, SP1, SP2, SP3
553 are given in **Table 2**.
554 The release probability for the simulation of IPSC variation was estimated with modified fitting
555 line of Figure. 4h in Holderith et al, 2012), y = 3.271 * 0.68 + 0.018. We multiplied slope of the
556 fitted line by 0.68 to get the similar release probability with pair cell recording result (**Figure. 8-**
557 **figure supplement 1**).
558
559 **Single cell electrophysiology experiment**
560 Experiments were performed as described for the electrophysiological recording experiments
561 previously (Kubota et al. 2007). Briefly, whole-cell access was obtained in neurons using visual
562 DIC optics and a 40x water immersion objective. The pipette solution consisted of (in mM):
563 potassium methylsulfate, 120; KCl, 5.0; EGTA, 0.5; $MgCl_2$, 1.7; $Na_2ATP$, 4.0; NaGTP, 0.3;
564 HEPES, 8.5; and biocytin, 17. The recording was usually performed for 10-20 minutes. After re-
565 slicing at 50 μm thickness, each slice (a set of 50 μm sections after resectioning) was further
566 treated by one of the following two procedures.
567 A. Some slices were incubated with avidin-biotin peroxidase complex (ABC) solution (Vector
568 Laboratory, Burlingame, CA, U.S.A.) in Tris-HCl buffered saline (TBS) with or without 0.04%
569 Triton X-100 (TX), and reacted with 3,3-diaminobenzidine tetrahydrochloride (DAB) (0.05%)
570 and $H_2O_2$ (0.003%) in 0.1 M phosphate buffer (PB).
571 B. Other slices were processed for fluorescence immunohistochemistry to identify

neurochemical markers, CRF and calretinin. The slices were incubated with the primary antibodies, CRF developed in rabbit (1:1000, gift by Dr. Wylie Vale, #PBLrC70) and calretinin (1:1000, Swant, Bellinzona, Switzerland, #6B3) in TBS containing 2% bovine serum albumin, 10% normal goat or horse serum and 0.04% TX. The slices were incubated in fluorescent secondary antibodies, followed by incubation with Alexa 350 streptavidin (1:200, Molecular Probes, Eugene, OR, U.S.A., #S-11249) in TBS. After examination for fluorescence, the slices were incubated with ABC, and reacted with DAB and $H_2O_2$.

Slices were then post-fixed in 1% $OsO_4$ in 0.1 M PB, dehydrated and flat embedded on silicon-coated glass slides in plastic (Epon 812 resin kit, TAAB, Aldermaston, U.K.). Recovered neurons were drawn using a drawing tube, or 3D reconstructed using the *Neurolucida* software (MBF Bioscience, Williston, VT, U.S.A.) attached to a NIKON ECLIPSE microscope equipped with a 60x objective lens (NIKON, Tokyo, Japan). After light microscopic reconstruction, stained cells were serially sectioned into 90nm thickness using an ultramicrotome (Reichert Ultracut S). Ultrathin sections mounted on one-hole grids were stained with lead citrate. Electron micrographs were taken with a Hitachi H-7000 electron microscope (EM), using tilting of up to 60˚. EM images of the labeled terminals and associated structures were captured using a CCD camera and reconstructed three-dimensionally (Visilog; Noesis, France).

**Statistics**

We used Mann Whitney U test (non-parametric) to compare the junctional area of somatic and dendritic/spine synapses (**Figure. 6F, G**) and Kolmogorov-Smirnov test to compare electric charge distributions from paired recordings experiment and the simulation of **Figure. 8 N, P**.

**Datasets**

The datasets I can provide are Neurolucida reconstructed neuron to the "NeuroMorpho.Org", http://neuromorpho.org/neuroMorpho/index.jsp, and authentic model cell for “Neuron” simulator to the “ModelDB”, https://senselab.med.yale.edu/modeldb. I believe these sites are standard public Neurolucida neuron file and model neuron sharing site. I will upload my files to those site after acceptance.

**Acknowledgments:**

We thank H. Kita and C. Shiozu for technical assistance and Dr. M. Ushimaru for helping to analyze the physiological data. We thank Drs. R. Miles and JL Chen for comments on the manuscript. This study was supported by the EM facility in National Institute for Physiological Sciences in Japan.

607 References and Notes:

608


609 Araya, R., J. Jiang, K. B. Eisenthal, and R. Yuste. 2006. "The spine neck filters membrane
610 potentials." *Proceedings of the National Academy of Sciences of the United States of*
611 *America* no. 103 (47):17961-6. doi: 10.1073/pnas.0608755103.
612 Bevan, M. D., C. J. Wilson, J. P. Bolam, and P. J. Magill. 2000. "Equilibrium potential of
613 GABA(A) current and implications for rebound burst firing in rat subthalamic neurons in
614 vitro." *Journal of neurophysiology* no. 83 (5):3169-72.
615 Buhl, E. H., K. Halasy, and P. Somogyi. 1994. "Diverse sources of hippocampal unitary
616 inhibitory postsynaptic potentials and the number of synaptic release sites." *Nature* no.
617 368 (6474):823-8. doi: 10.1038/368823a0.
618 Chen, J. L., K. L. Villa, J. W. Cha, P. T. So, Y. Kubota, and E. Nedivi. 2012. "Clustered
619 dynamics of inhibitory synapses and dendritic spines in the adult neocortex." *Neuron* no.
620 74 (2):361-73. doi: 10.1016/j.neuron.2012.02.030.
621 Chen, T. W., T. J. Wardill, Y. Sun, S. R. Pulver, S. L. Renninger, A. Baohan, E. R. Schreiter, R.
622 A. Kerr, M. B. Orger, V. Jayaraman, L. L. Looger, K. Svoboda, and D. S. Kim. 2013.
623 "Ultrasensitive fluorescent proteins for imaging neuronal activity." *Nature* no. 499
624 (7458):295-300. doi: 10.1038/nature12354.
625 Chiu, C. Q., G. Lur, T. M. Morse, N. T. Carnevale, G. C. Ellis-Davies, and M. J. Higley. 2013.
626 "Compartmentalization of GABAergic inhibition by dendritic spines." *Science* no. 340
627 (6133):759-62. doi: 10.1126/science.1234274.
628 Cossart, R., C. Dinocourt, J. C. Hirsch, A. Merchan-Perez, J. De Felipe, Y. Ben-Ari, M.
629 Esclapez, and C. Bernard. 2001. "Dendritic but not somatic GABAergic inhibition is
630 decreased in experimental epilepsy." *Nature neuroscience* no. 4 (1):52-62. doi:
631 10.1038/82900.
632 Donato, F., A. Chowdhury, M. Lahr, and P. Caroni. 2015. "Early- and late-born parvalbumin
633 basket cell subpopulations exhibiting distinct regulation and roles in learning." *Neuron*
634 no. 85 (4):770-86. doi: 10.1016/j.neuron.2015.01.011.
635 Donato, F., S. B. Rompani, and P. Caroni. 2013. "Parvalbumin-expressing basket-cell network
636 plasticity induced by experience regulates adult learning." *Nature* no. 504 (7479):272-6.
637 doi: 10.1038/nature12866.
638 Fiala, J. C. 2005. "Reconstruct: a free editor for serial section microscopy." *Journal of*
639 *microscopy* no. 218 (Pt 1):52-61. doi: 10.1111/j.1365-2818.2005.01466.x.
640 Fino, E., and R. Yuste. 2011. "Dense inhibitory connectivity in neocortex." *Neuron* no. 69
641 (6):1188-203. doi: 10.1016/j.neuron.2011.02.025.
642 Fleidervish, I. A., and L. Libman. 2008. "How cesium dialysis affects the passive properties of
643 pyramidal neurons: implications for voltage clamp studies of persistent sodium current."
644 *New Journal of Physics* no. 10 (3):035001. doi: 10.1088/1367-2630/10/3/035001.
645 Gibson, J. R., M. Beierlein, and B. W. Connors. 1999. "Two networks of electrically coupled
646 inhibitory neurons in neocortex." *Nature* no. 402 (6757):75-9. doi: 10.1038/47035.
647 Gidon, A., and I. Segev. 2012. "Principles governing the operation of synaptic inhibition in
648 dendrites." *Neuron* no. 75 (2):330-41. doi: 10.1016/j.neuron.2012.05.015.
649 Gonzalez-Burgos, G., T. Hashimoto, and D. A. Lewis. 2010. "Alterations of cortical GABA
650 neurons and network oscillations in schizophrenia." *Current psychiatry reports* no. 12
651 (4):335-44. doi: 10.1007/s11920-010-0124-8.

Gulledge, A. T., N. T. Carnevale, and G. J. Stuart. 2012. "Electrical advantages of dendritic spines." *PloS one* no. 7 (4):e36007. doi: 10.1371/journal.pone.0036007.
Gulledge, A. T., and G. J. Stuart. 2003. "Excitatory actions of GABA in the cortex." *Neuron* no. 37 (2):299-309.
Hao, J., X. D. Wang, Y. Dan, M. M. Poo, and X. H. Zhang. 2009. "An arithmetic rule for spatial summation of excitatory and inhibitory inputs in pyramidal neurons." *Proceedings of the National Academy of Sciences of the United States of America* no. 106 (51):21906-11. doi: 10.1073/pnas.0912022106.
Harnett, M. T., J. K. Makara, N. Spruston, W. L. Kath, and J. C. Magee. 2012. "Synaptic amplification by dendritic spines enhances input cooperativity." *Nature* no. 491 (7425):599-602. doi: 10.1038/nature11554.
Hensch, T. K. 2005. "Critical period plasticity in local cortical circuits." *Nature reviews. Neuroscience* no. 6 (11):877-88. doi: 10.1038/nrn1787.
Hines, M. L., and N. T. Carnevale. 1997. "The NEURON simulation environment." *Neural computation* no. 9 (6):1179-209.
Holderith, N., A. Lorincz, G. Katona, B. Rozsa, A. Kulik, M. Watanabe, and Z. Nusser. 2012. "Release probability of hippocampal glutamatergic terminals scales with the size of the active zone." *Nature neuroscience* no. 15 (7):988-97. doi: 10.1038/nn.3137.
Isomura, Y., R. Harukuni, T. Takekawa, H. Aizawa, and T. Fukai. 2009. "Microcircuitry coordination of cortical motor information in self-initiation of voluntary movements." *Nature neuroscience* no. 12 (12):1586-93. doi: 10.1038/nn.2431.
Jiang, X., G. Wang, A. J. Lee, R. L. Stornetta, and J. J. Zhu. 2013. "The organization of two new cortical interneuronal circuits." *Nature neuroscience* no. 16 (2):210-8. doi: 10.1038/nn.3305.
Karube, F., Y. Kubota, and Y. Kawaguchi. 2004. "Axon branching and synaptic bouton phenotypes in GABAergic nonpyramidal cell subtypes." *The Journal of neuroscience : the official journal of the Society for Neuroscience* no. 24 (12):2853-65. doi: 10.1523/JNEUROSCI.4814-03.2004.
Katz, Y., V. Menon, D. A. Nicholson, Y. Geinisman, W. L. Kath, and N. Spruston. 2009. "Synapse distribution suggests a two-stage model of dendritic integration in CA1 pyramidal neurons." *Neuron* no. 63 (2):171-7. doi: 10.1016/j.neuron.2009.06.023.
Kawaguchi, Y., and Y. Kubota. 1998. "Neurochemical features and synaptic connections of large physiologically-identified GABAergic cells in the rat frontal cortex." *Neuroscience* no. 85 (3):677-701.
Kimura, F., C. Itami, K. Ikezoe, H. Tamura, I. Fujita, Y. Yanagawa, K. Obata, and M. Ohshima. 2010. "Fast activation of feedforward inhibitory neurons from thalamic input and its relevance to the regulation of spike sequences in the barrel cortex." *The Journal of physiology* no. 588 (Pt 15):2769-87. doi: 10.1113/jphysiol.2010.188177.
Kisvarday, Z. F., K. A. Martin, D. Whitteridge, and P. Somogyi. 1985. "Synaptic connections of intracellularly filled clutch cells: a type of small basket cell in the visual cortex of the cat." *The Journal of comparative neurology* no. 241 (2):111-37. doi: 10.1002/cne.902410202.
Klausberger, T., and P. Somogyi. 2008. "Neuronal diversity and temporal dynamics: the unity of hippocampal circuit operations." *Science* no. 321 (5885):53-7. doi: 10.1126/science.1149381.

Knott, G. W., C. Quairiaux, C. Genoud, and E. Welker. 2002. "Formation of dendritic spines with GABAergic synapses induced by whisker stimulation in adult mice." *Neuron* no. 34 (2):265-73.
Kubota, Y. 2014. "Untangling GABAergic wiring in the cortical microcircuit." *Current opinion in neurobiology* no. 26:7-14. doi: 10.1016/j.conb.2013.10.003.
Kubota, Y., S. Hatada, S. Kondo, F. Karube, and Y. Kawaguchi. 2007. "Neocortical inhibitory terminals innervate dendritic spines targeted by thalamocortical afferents." *The Journal of neuroscience : the official journal of the Society for Neuroscience* no. 27 (5):1139-50. doi: 10.1523/JNEUROSCI.3846-06.2007.
Kubota, Y., F. Karube, M. Nomura, A. T. Gulledge, A. Mochizuki, A. Schertel, and Y. Kawaguchi. 2011. "Conserved properties of dendritic trees in four cortical interneuron subtypes." *Scientific reports* no. 1:89. doi: 10.1038/srep00089.
Kubota, Y., and Y. Kawaguchi. 2000. "Dependence of GABAergic synaptic areas on the interneuron type and target size." *The Journal of neuroscience : the official journal of the Society for Neuroscience* no. 20 (1):375-86.
Kubota, Y., N. Shigematsu, F. Karube, A. Sekigawa, S. Kato, N. Yamaguchi, Y. Hirai, M. Morishima, and Y. Kawaguchi. 2011. "Selective coexpression of multiple chemical markers defines discrete populations of neocortical GABAergic neurons." *Cerebral cortex* no. 21 (8):1803-17. doi: 10.1093/cercor/bhq252.
Larkman, A., and A. Mason. 1990. "Correlations between morphology and electrophysiology of pyramidal neurons in slices of rat visual cortex. I. Establishment of cell classes." *The Journal of neuroscience : the official journal of the Society for Neuroscience* no. 10 (5):1407-14.
Larkum, M. E., T. Nevian, M. Sandler, A. Polsky, and J. Schiller. 2009. "Synaptic integration in tuft dendrites of layer 5 pyramidal neurons: a new unifying principle." *Science* no. 325 (5941):756-60. doi: 10.1126/science.1171958.
Lee, S. H., A. C. Kwan, S. Zhang, V. Phoumthipphavong, J. G. Flannery, S. C. Masmanidis, H. Taniguchi, Z. J. Huang, F. Zhang, E. S. Boyden, K. Deisseroth, and Y. Dan. 2012. "Activation of specific interneurons improves V1 feature selectivity and visual perception." *Nature* no. 488 (7411):379-83. doi: 10.1038/nature11312.
Lee, S. H., I. Marchionni, M. Bezaire, C. Varga, N. Danielson, M. Lovett-Barron, A. Losonczy, and I. Soltesz. 2014. "Parvalbumin-Positive Basket Cells Differentiate among Hippocampal Pyramidal Cells." *Neuron* no. 82 (5):1129-44. doi: 10.1016/j.neuron.2014.03.034.
Liu, G. 2004. "Local structural balance and functional interaction of excitatory and inhibitory synapses in hippocampal dendrites." *Nature neuroscience* no. 7 (4):373-9. doi: 10.1038/nn1206.
Magee, J. C. 2000. "Dendritic integration of excitatory synaptic input." *Nature reviews. Neuroscience* no. 1 (3):181-90. doi: 10.1038/35044552.
Marlin, J. J., and A. G. Carter. 2014. "GABA-A Receptor Inhibition of Local Calcium Signaling in Spines and Dendrites." *The Journal of neuroscience : the official journal of the Society for Neuroscience* no. 34 (48):15898-911. doi: 10.1523/JNEUROSCI.0869-13.2014.
Matsuzaki, M., N. Honkura, G. C. Ellis-Davies, and H. Kasai. 2004. "Structural basis of long-term potentiation in single dendritic spines." *Nature* no. 429 (6993):761-6. doi: 10.1038/nature02617.

Meguro, R., R. Hishida, H. Tsukano, K. Yoshitake, R. Imamura, M. Tohmi, T. Kitsukawa, T. Hirabayashi, T. Yagi, H. Takebayashi, and K. Shibuki. 2015. "Impaired clustered protocadherin-alpha leads to aggregated retinogeniculate terminals and impaired visual acuity in mice." *Journal of neurochemistry* no. 133 (1):66-72. doi: 10.1111/jnc.13053.

Miles, R., K. Toth, A. I. Gulyas, N. Hajos, and T. F. Freund. 1996. "Differences between somatic and dendritic inhibition in the hippocampus." *Neuron* no. 16 (4):815-23.

Morishima, M., and Y. Kawaguchi. 2006. "Recurrent connection patterns of corticostriatal pyramidal cells in frontal cortex." *The Journal of neuroscience : the official journal of the Society for Neuroscience* no. 26 (16):4394-405. doi: 10.1523/JNEUROSCI.0252-06.2006.

Morishima, M., K. Morita, Y. Kubota, and Y. Kawaguchi. 2011. "Highly differentiated projection-specific cortical subnetworks." *The Journal of neuroscience : the official journal of the Society for Neuroscience* no. 31 (28):10380-91. doi: 10.1523/JNEUROSCI.0772-11.2011.

Nakamura, Y., H. Harada, N. Kamasawa, K. Matsui, J. S. Rothman, R. Shigemoto, R. A. Silver, D. A. DiGregorio, and T. Takahashi. 2015. "Nanoscale distribution of presynaptic Ca(2+) channels and its impact on vesicular release during development." *Neuron* no. 85 (1):145-58. doi: 10.1016/j.neuron.2014.11.019.

Nusser, Z., S. Cull-Candy, and M. Farrant. 1997. "Differences in synaptic GABA(A) receptor number underlie variation in GABA mini amplitude." *Neuron* no. 19 (3):697-709.

Packer, A. M., D. J. McConnell, E. Fino, and R. Yuste. 2013. "Axo-dendritic overlap and laminar projection can explain interneuron connectivity to pyramidal cells." *Cerebral cortex* no. 23 (12):2790-802. doi: 10.1093/cercor/bhs210.

Packer, A. M., and R. Yuste. 2011. "Dense, unspecific connectivity of neocortical parvalbumin-positive interneurons: a canonical microcircuit for inhibition?" *The Journal of neuroscience : the official journal of the Society for Neuroscience* no. 31 (37):13260-71. doi: 10.1523/JNEUROSCI.3131-11.2011.

Puig, M. V., M. Ushimaru, and Y. Kawaguchi. 2008. "Two distinct activity patterns of fast-spiking interneurons during neocortical UP states." *Proceedings of the National Academy of Sciences of the United States of America* no. 105 (24):8428-33. doi: 10.1073/pnas.0712219105.

Pulido, C., F. F. Trigo, I. Llano, and A. Marty. 2015. "Vesicular release statistics and unitary postsynaptic current at single GABAergic synapses." *Neuron* no. 85 (1):159-72. doi: 10.1016/j.neuron.2014.12.006.

Rubenstein, J. L., and M. M. Merzenich. 2003. "Model of autism: increased ratio of excitation/inhibition in key neural systems." *Genes, brain, and behavior* no. 2 (5):255-67.

Sasaki, T., N. Matsuki, and Y. Ikegaya. 2012. "Heterogeneity and independency of unitary synaptic outputs from hippocampal CA3 pyramidal cells." *The Journal of physiology*. doi: 10.1113/jphysiol.2012.237685.

Sauer, J. F., M. Struber, and M. Bartos. 2015. "Impaired fast-spiking interneuron function in a genetic mouse model of depression." *eLife* no. 4. doi: 10.7554/eLife.04979.

Silberberg, G., and H. Markram. 2007. "Disynaptic inhibition between neocortical pyramidal cells mediated by Martinotti cells." *Neuron* no. 53 (5):735-46. doi: 10.1016/j.neuron.2007.02.012.

786 Stuart, G. J., H. U. Dodt, and B. Sakmann. 1993. "Patch-clamp recordings from the soma and
787 dendrites of neurons in brain slices using infrared video microscopy." *Pflugers Archiv :*
788 *European journal of physiology* no. 423 (5-6):511-8.
789 Szabadics, J., C. Varga, G. Molnar, S. Olah, P. Barzo, and G. Tamas. 2006. "Excitatory effect of
790 GABAergic axo-axonic cells in cortical microcircuits." *Science* no. 311 (5758):233-5.
791 doi: 10.1126/science.1121325.
792 Tanaka, J., M. Matsuzaki, E. Tarusawa, A. Momiyama, E. Molnar, H. Kasai, and R. Shigemoto.
793 2005. "Number and density of AMPA receptors in single synapses in immature
794 cerebellum." *The Journal of neuroscience : the official journal of the Society for*
795 *Neuroscience* no. 25 (4):799-807. doi: 10.1523/JNEUROSCI.4256-04.2005.
796 Verheugen, J. A., D. Fricker, and R. Miles. 1999. "Noninvasive measurements of the membrane
797 potential and GABAergic action in hippocampal interneurons." *The Journal of*
798 *neuroscience : the official journal of the Society for Neuroscience* no. 19 (7):2546-55.
799 Xue, M., B. V. Atallah, and M. Scanziani. 2014. "Equalizing excitation-inhibition ratios across
800 visual cortical neurons." *Nature* no. 511 (7511):596-600. doi: 10.1038/nature13321.
801 Yagi, T. . 2015. "Protocadherins in mammalian neuronal individuality and connectivity.
802 " In *Neural Surface Antigens: FROM BASIC BIOLOGY TOWARDS BIOMEDICAL*
803 *APPLICATIONS*, edited by J. Pruszak, 141-152. Oxford, U.K.: Elsevier.
804 Yee, K. T., H. H. Simon, M. Tessier-Lavigne, and D. M. O'Leary. 1999. "Extension of long
805 leading processes and neuronal migration in the mammalian brain directed by the
806 chemoattractant netrin-1." *Neuron* no. 24 (3):607-22.
807 Yoshimura, Y., J. L. Dantzker, and E. M. Callaway. 2005. "Excitatory cortical neurons form
808 fine-scale functional networks." *Nature* no. 433 (7028):868-73. doi:
809 10.1038/nature03252.
810
811
812

## Figures

### Figure. 1

Paired recording between FS basket cells and CCS pyramidal cells in L5.

**A-E** Structural and functional characteristics of pair CS28. **A.** The presynaptic FS basket cell shows a fast-spiking (upper left) and the postsynaptic pyramidal cell displayed a regular spiking behavior (bottom left). Average IPSC response in the pyramidal cell (bottom right) to a single AP elicited in the FS basket cell (upper right). **B.** Reconstruction of the neuron pair. The somatodendritic domain of the presynaptic FS basket cell is shown in blue, the axonal arborization in sky blue, and the somatodendritic domain of the postsynaptic pyramidal cell in gray. **C.** Illustration showing the number and distribution of putative synaptic contacts (red dots) established by the FS basket cell axonal collaterals on the soma and proximal dendritic segments of the postsynaptic pyramidal cell. **D.** LMg of the pyramidal cell soma with its inhibitory synaptic contacts (arrows) illustrated in (**C**). **E.** Dendrogram of the pyramidal cell basal dendrite with putative contact sites (red bars). **F-I**. Structural and functional characteristics of pair CS45. **F.** Averaged IPSC in the pyramidal cell in response to a single action potential in the presynaptic FS basket cell. **G.** Reconstruction of the cell pair. Same color code as in (**B**) with putative synaptic contacts (red). Note that synaptic contacts were exclusively found on dendrites. **H.** Low power LMg of the cell pair showing a putative contact site on the basal dendrite of the pyramidal cell (red arrow) by the FS basket cell axon at low (left panel) and high (right panel) magnification. **I.** Dendrogram of the basal dendrites of the pyramidal cell with ten LM-identified contact sites (red bars). **J.** Summary diagram showing the number and distribution of putative contacts established on postsynaptic pyramidal cell somata and dendrites for all investigated pairs. The corresponding averaged IPSC peak amplitude is shown on the right. For the last 2 pairs, no IPSCs were detectable despite the presence of LM-identified contact sites.

**Figure. 1-figure supplement 1**

The CCS pyramidal cell in layer V identified by retrograde fluorescent tracer.

**A**. Cholera toxin subunit B (CTB) conjugated with Alexa-555 fluorescent tracer was injected into contra-lateral striatum. **B.** Subpopulation of layer V pyramidal cells were labeled with the fluorescent tracer in ipsilateral cortex. **C.** Enlarged image of dotted square in (**B**). Many labeled layer V CCS pyramidal cells are seen.

**Figure. 1-figure supplement 2**

Physiological properties of IPSCs evoked in CCS pyramidal cells in L5, related to Figure 1.

**A**. Presynaptic FS basket cell AP (upper trace) and the evoked IPSC in the postsynaptic pyramidal cell (bottom trace). Fitting lines are shown for rise (red) and decay phase (blue) of the IPSC. **B**. Bar histogram of the distribution of IPSC amplitudes and noise. **C**. IPSC traces at several somatic holding membrane potential (upper traces) and corresponding diagram showing the relationship of the IPSC amplitude to membrane potential (bottom). The reversal potential is -52.5 mV determined by a linear fit of the plot. **D**. Bar histograms of the latency, **E**. rise time, **F**. decay time constant, and **G**. success rates of IPSCs in the postsynaptic pyramidal cell.

**Figure. 2**

Different unitary IPSCs induced by single FS basket cells in L5 CCS pyramidal cells.

**A.** Pre-synaptic basket cell and post-synaptic pyramidal cell. Light micrograph (LMg) of the CS56 pair. Scale bar: 100 μm, as in (**F**). **B.** Reconstruction of pyramidal cell soma-dendrites (blue) and axon (sky blue), basket cell soma-dendrites (red) and axon (pink). **C.** Close-up of the

pyramidal cell soma. Scale bar, 10 μm. **D.** Putative synaptic contacts (blue bars) shown on dendrogram including basal (gray) and apical (sky blue) dendrites. **E.** Maximum (left) and averaged (right) IPSCs evoked by single FS basket cell spikes. **F.** Pre-synaptic basket cell and post-synaptic pyramidal cell. LMg of CS55 pair. **G.** Reconstruction. **H.** Close-up of the pyramidal cell soma. **I.** Dendrogram with putative synaptic contact sites (blue bar). **J.** Maximum (left) and average (right) IPSCs evoked by single FS basket cell APs.

**Figure. 2-figure supplement 1**

Drawings of the paired recording between FS basket cells and CCS pyramidal cells in L5. Postsynaptic pyramidal cell soma-dendrites (blue) and axon (sky blue), presynaptic FS basket cell soma-dendrites (red) and axon (pink) are shown.

**Figure. 2-figure supplement 2**

Sholl analysis of presynaptic FS basket cell axon to postsynaptic CCS pyramidal cell soma center.

**A**. Sholl analysis showing entire FS basket cell axon fiber arborization. **B**. The initial part up to 20 μm from soma is enlarged to see the difference in terms of the intersections between the cell pairs.

**Figure. 3**

3D reconstruction from serial EMgs.

**A.** *Neurolucida* reconstruction of the postsynaptic pyramidal cell of the CS56 pair. A dendritic segments (C1) is marked in red and red arrow. **B.** Corresponding LMg of the dendritic segment C1 (focus stack image). The FS basket cell axon terminal is indicated by arrow. **C.** EMgs from

three adjacent ultrathin sections of segment C1. **D.** 3D reconstruction of the dendritic segment C1. The FS basket cell axon (red) did not establish a synaptic contact with the dendritic segment C1 (red arrow). Scale bar in (**B**) is the same for (**D**).

**Figure. 3-figure supplement 1**

Focus step images for C1 dendritic segment with FS cell axonal fiber contact site shown in Figure. 2B.

**A-F.** The dendritic segment images of every 0.5 μm focus step were captured. The focus stacking LMg of Figure. 2B was composed of focused area of these images.

**Figure. 4**

Dendritic segments and the somatic region selected for further quantitative EM analysis.

Dendrogram of the apical (left) and basal (right) dendrites of the postsynaptic pyramidal cell of pair CS56. Dendritic segments indicated by red circles and numbers and the somatic region (inset grey drawing) were selected and analyzed in serial ultrathin sections at the EM level. In this pair seven synaptic contact sites were identified at the light microscopic level (C1-C7).

**Figure. 5**

EM identification of synaptic contacts.

**A.** LMg of putative synaptic contacts (white arrows) made by a basket cell on the soma of a pyramidal cell of CS56. **B-D.** EMgs of three somatic synaptic contacts (S1-S3). Thick arrows indicate synaptic junctions, small arrows the extremities of the synaptic cleft. **E.** The upper view is 3D reconstruction of somatic synapses (red) on soma (green) in the same plane as **A**, the

middle image, rotated by 90°, shows three boutons apposed to the pyramidal cell soma and the lower view shows their synaptic junctions. **F.** LMg of putative synaptic contacts on a pyramidal cell dendrite. **G.** EM of synapses with a dendritic spine (Sp1, upper left arrow) and dendritic shaft (D1, bottom right arrow) 40 degree tilting angle. **H.** EMg of the spine synapse in **G** (arrow). **I.** 3D reconstructions of the synapses in **G**. Lower left image shows the dendritic segment indicated by arrows in (**F**). Middle view, rotated by ~60°, shows the junction made with the spine (red). Right image is rotated by ~-90° to visualize the junction on the dendrite. **J**. Focus stack image of LMg of putative contacts (arrows) made by basket cell axonal terminals on a pyramidal cell soma and dendrites of CS55. **K, L.** EM of the S6 **(K)** and S7 **(L)** somatic junctions. **M, N.** Two views of a 3D reconstruction of a FS cell axon (red) and pyramidal cell soma (green) showing all contacts. (at, axon terminal; sp, spine; dend, dendrite)

**Figure. 5-figure supplement 1**

Somatic synapse contact sites identified using electron microscopic observation.

**A.** Light micrograph showing FS cell axon terminal contacting to the postsynaptic pyramidal cell soma (arrow). The axon terminal looks just a hump of the somatic surface under the light microscope. **B.** Electron micrograph showing the somatic synapse of the FS cell axon terminal contacting to the pyramidal cell soma (arrow). At: axon terminal. **C.** 3D reconstruction images of the somatic synapse. Upper image is in the same angle as the light micrograph in **(A)**. Bottom left image is 90 degree rotated image showing soma surface (green). Bottom right image shows synaptic junction.

**Figure. 5-figure supplement 2**

Focus step images for CS55 pair neurons shown in Figure. 3J.

**A-Y.** The somatic, dendritic segment and axonal fiber images of every 0.5 μm focus step were captured. The focus stacking LMg of Figure. 3J was composed of focused area in these images.

**Figure. 5-figure supplement 3**

The presynaptic FS basket cell axon terminal crosses the postsynaptic pyramidal cell CS55 dendrite. **A**. Focus stack image of LMg of putative contacts made by the FS basket cell axonal terminal on the pyramidal cell dendrite (C9, arrow). This contact was not verified with EM. The other presynaptic fiber is accessing to the pyramidal cell soma (white arrow). The presynaptic axon terminals contact on the other cell soma (arrows). **B**. Focus stack image of LMg of putative contacts made by the FS basket cell axonal terminal on a pyramidal cell dendrite (C8, arrow). This contact was not verified with EM.

**Figure. 6**

Synapse contact sites identified by EM observation of pairs CS56 and CS55. **A, B.** Synaptic contact sites are shown in drawings of CS56 pair neurons (**A**) and CS55 pair neurons (**B**). Postsynaptic pyramidal cell soma and dendrites are in blue, presynaptic FS basket cell soma and dendrites are in red, and axon in pink. **C, D.** The synapse contact sites are shown in dendrograms of the basal dendrites of postsynaptic pyramidal cell of CS56 pair (**C**) and CS55 pair (**D**). **E.** Distribution of putative synaptic contacts (black bars) made by single basket cells on somato-dendritic membrane of 10 pyramidal cells. Contacts confirmed by EM are shown in red. **F, G.** Area of somatic synaptic junctions is significantly larger than those on dendritic shafts and spines of CS56 pair neurons (**F**) and CS55 pair neurons (**G**).

**Figure. 6-figure supplement 1**

Linear correlation of synapse junction area and bouton volume.

**A, B**. Diagram showing the positive linear correlation of synapse junction area and bouton volume of CS56 (**A**) and CS55 (**B**).

**Figure. 7**

Schematic summary.

Schematic drawing to summarize our main findings.

**Figure. 8**

Simulated conduction for dendritic spine, shaft and somatic IPSCs. **A-C.** Dendro-somatic conduction of a spine synapse IPSC. **A.** Peak membrane potential changes (color-coded as in (**M)**) over somato-dendritic membrane induced by an IPSC of 0.11 nS injected at Sp1 of the model pyramidal cell (red arrow). Peak inhibitory potential of the spine in red. **B** IPSC waveform injected at Sp1 spine head is reduced to 64% at the soma. **C.** Simulated IPSPs. Current flow indicated by arrows. IPSP attenuation was 15% at the basal dendrite and 9% at the soma. **D-F.** Conduction of a dendritic shaft IPSC, D1. **d.** Peak somato-dendritic potential changes induced by an IPSC of amplitude 0.21 nS injected at a dendritic shaft (red arrow). **E.** IPSC waveform injected at D1 (upper) and simulated somatic IPSC (lower trace) with an attenuation of 63%. **F.** IPSP wave form. Current flow indicated by arrows. IPSP attenuation at the soma is 57%, but no attenuation at the spine. **G, H. C**onduction of a somatic IPSC, S1. **G.** Peak somato-dendritic potential changes induced by an IPSC of amplitude 0.7 nS injected at the S1 somatic site (red arrow). **H.** IPSC waveform injected at S1 (upper) resulting in a somatic IPSP (lower). **I.** Somato-dendritic conduction of the IPSC resulting from activating (red arrow) four somatic synapses S1,

S2, S3 and S4. **J.** Summed IPSC waveform (upper trace, S1-S4) and somatic IPSP (lower). **K.** Peak somatic IPSPs for 8 different injected IPSCs. **L.** Reduction (green) of the EPSP resulting from the injection of an EPSC waveform of 0.2 nS (red) at the spine head, Sp1, by an IPSC (blue) injected at the same site and time. **M.** Color-coded dendrogram and corresponding somatic synaptic contacts on the model cell. **N.** Bar histogram showing the distribution of IPSC electric charge of the pair CS56. **O.** IPSC variance and the average IPSC of the pair CS56. **P.** Bar histogram of the distribution of IPSC electric charge when simulated. Here, the IPSC electric charge also substantially varied from trial to trial and is not significantly different as in the paired recording (Kolmogorov-Smirnov test, p= 0.41).

**Figure. 8-figure supplement 1**

Relationship showing synapse conductance and release probability used for simulation analysis in Figure. 6P.

**Figure. 9**

Dendrograms with contact sites of the post synaptic pyramidal cells

Individual dendrograms of all investigated postsynaptic pyramidal cells (n=10). Apical dendrograms are shown in blue and basal dendrograms are in gray.

**Figure. 10**

Linear correlation between synapse junction area and postsynaptic target size of non-pyramidal cells. **A.** Different types of cortical GABAergic non-pyramidal cells. The somatodendritic domain of the neurons is given in black and their axons in red. Abbreviations: LS, late spiking cell; FS, fast spiking cell; BSNP, burst spiking non-pyramidal cell; RSNP, regular spiking non-pyramidal cell; CR, calretinin; CRF, corticotropin releasing factor. **B, C.** 3D reconstructions of synaptic junctions (red) on target structures (green) of inhibitory axon terminals by cortical FS basket cell (**B**) and descending basket BSNP-CR cell (**C**) using 3D serial EMgs. The thickness of the target structure (from left to right) is positively correlated to the size of the junction area. **D-L.** Line diagrams correlating synaptic junction area of the non-pyramidal neurons with spine head volume (left panel), dendrite cross sectional area (middle panel) and plots with soma (right panel). The synapse junction area on spines and dendrites is linearly correlated with the target size. The somatic synapse is larger when compared with dendritic and spine synapse.

## Tables

Table 1 Synapse properties of pair recordings

| | Amplitude | | | | | |
|---|---|---|---|---|---|---|
| | mean (pA) | sd (pA) | max (pA) | success rate | Neurolucida analysis | soma distance (μm) |
| IPSC | | | | | | |
| CS4 | -5.7 | 5.1 | -19.5 | 0.6 | | |
| CS8 | -8.6 | 4.0 | -17.6 | 0.5 | yes | 48.8 |
| CS20 | -10.9 | 5.3 | -27.4 | 0.9 | yes | 51.8 |
| CS21* | -7.6 | 3.2 | -17.8 | 0.6 | | |
| CS22* | -8.0 | 3.4 | -14.5 | 0.6 | | |
| CS28 | -76.9 | 20.9 | -107.3 | 1.0 | yes | 48.8 |
| CS36* | -6.5 | 2.6 | -12.5 | 0.4 | | |
| CS41 | -8.6 | 4.3 | -20.8 | 0.7 | yes | 41.3 |
| CS44 | -6.2 | 2.1 | -12.6 | 0.5 | yes | 66.6 |
| CS45* | -7.1 | 4.1 | -21.2 | 0.7 | yes | 53.2 |
| CS55 | -91.3 | 11.2 | -111.0 | 1.0 | yes | 35.8 |
| CS56 | -17.3 | 3.0 | -24.9 | 1.0 | yes | 20.6 |
| CS61 | -9.6 | 4.6 | -22.2 | 0.8 | | |
| CS62 | -36.4 | 14.0 | -69.5 | 1.0 | | |
| EPSC | | | | | | |
| CS10 | 67.5 | 22.2 | 109.3 | 1.0 | yes | 26.5 |
| CS21* | 18.6 | 8.7 | 44.5 | 0.9 | | |
| CS22* | 70.9 | 38.3 | 201.6 | 1.0 | | |
| CS23 | 45.3 | 14.2 | 83.4 | 1.0 | yes | 51.2 |
| CS36* | 4.4 | 1.0 | 6.5 | 0.5 | | |
| CS45* | 43.1 | 19.0 | 86.1 | 1.0 | yes | 53.2 |

* Reciprocal connection between FS and pyramidal cell was observed.

Table 2 Synapse properties of pair CS56

| synapse | target | junction area (m2) | electric charge (fC)* | conductance (nS) † | distance from soma (m) |
|---|---|---|---|---|---|
| S1 | soma | 0.350 | 120.1 | 0.71 | 0 |
| S2 | soma | 0.174 | 59.7 | 0.35 | 0 |
| S3 | soma | 0.194 | 66.6 | 0.39 | 0 |
| S4 | soma | 0.232 | 79.6 | 0.47 | 0 |
| sub total | | 0.950 | | | |
| D1 | dendrite | 0.102 | 35.2 | 0.21 | 34 |
| Sp1 | spine | 0.056 | 19.2 | 0.11 | 34 |
| Sp2 | spine | 0.051 | 17.6 | 0.10 | 83 |
| Sp3 | spine | 0.042 | 14.4 | 0.08 | 106 |

* estimated from junctional area, † estimated from electric charge"

Table 3 Synapse properties of pair CS55

| synapse | target | junction area (m2) | electric charge (fC)* | distance from soma (m) |
|---|---|---|---|---|
| S1 | soma | 0.116 | 40.9 | 0 |
| S2 | soma | 0.221 | 77.6 | 0 |
| S3 | soma | 0.052 | 18.4 | 0 |
| S4 | soma | 0.120 | 42.3 | 0 |
| S5 | soma | 0.436 | 153.0 | 0 |
| S6 | soma | 0.194 | 68.2 | 0 |
| S7 | soma | 0.344 | 121.0 | 0 |
| S8 | soma | 0.151 | 52.9 | 0 |
| S9 | soma | 0.068 | 23.8 | 0 |
| S10 | soma | 0.138 | 48.3 | 0 |
| S11 | soma | 0.132 | 46.2 | 0 |
| S12 | soma | 0.211 | 74.1 | 0 |
| S13 | somatic spine | 0.092 | 32.3 | 0 |
| sub total | | 2.274 | | |
| D1 | dendrite | 0.044 | 15.3 | 6 |
| D2 | dendrite | 0.176 | 61.8 | 8.6 |
| Sp1 | spine | 0.180 | 63.2 | 12.6 |
| D3 | dendrite | 0.058 | 20.3 | 22.6 |
| Sp2 | spine | 0.054 | 19.1 | 22.6 |
| D4 | dendrite | 0.060 | 21.1 | 24.7 |
| Sp3 | spine | 0.099 | 34.6 | 24.9 |
| Sp4 | spine | 0.067 | 23.4 | 24.9 |
| sub total | | 3.011 | | |
| D5 | dendrite | 0.055 | 19.3 | 44.8 |
| D6 | dendrite | 0.060 | 21.1 | 84.5 |
| D7 | dendrite | 0.046 | 16.2 | 188.5 |

* estimated from junctional area

Table 4 Proportion of basket terminal

| pair | bouton | basket terminal | total bouton | basket terminal (%) |
|---|---|---|---|---|
| CS55 | 179 | 106 | 285 | 37.2 |
| CS28 | - | - | - | - |
| CS56 | 120 | 91 | 211 | 43.1 |
| CS20 | 165 | 52 | 217 | 24.0 |
| CS41 | 175 | 73 | 248 | 29.4 |
| CS8 | 142 | 59 | 201 | 29.4 |
| CS45 | 125 | 26 | 151 | 17.2 |
| CS44 | 166 | 67 | 233 | 28.8 |
| CS10 | 167 | 59 | 226 | 26.1 |
| CS23 | 252 | 63 | 315 | 20.0 |
| total/average | 1491 | 596 | 2087 | 28.4 ± 7.6 |

Table 5 IPSC properties of pair CS56 and CS55

| | CS56 | | CS55 | |
|---|---|---|---|---|
| | electric charge (fC) | peak (pA) | electric charge (fC) | peak (pA) |
| Average | 193.1 | -17.3 | 895.2 | -91.3 |
| SD | 56.2 | 3.0 | 96.2 | 11.2 |
| Max | 326.1 | -24.9 | 1057.8 | -111.0 |
| Min | 89.9 | -11.8 | 766.0 | -74.0 |
| n | 60 | 60 | 10 | 10 |
| Average Trace | 217.5 | -14.2 | 994.6 | -89.4 |

Table 6  Unit IPSC

| pair | electric charge (fC) | junction area (_m2) | Unit IPSC (fC/(_m2) |
|---|---|---|---|
| CS56 | 326.1 | 0.950 | 343.3 |
| CS55 | 1057.8 | 3.011 | 351.3 |

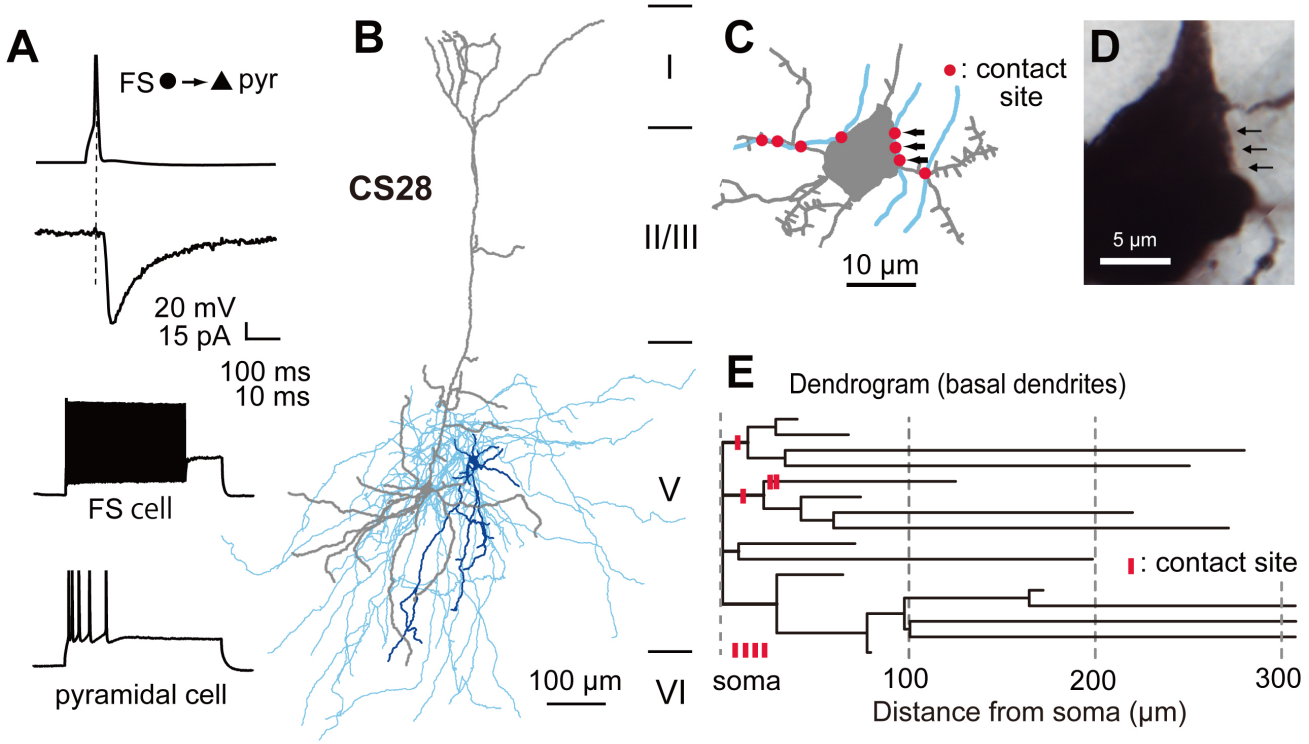
A
FS ● → ▲ pyr
20 mV
15 pA
100 ms
10 ms
FS cell
pyramidal cell
B
CS28
I
II/III
V
VI
100 µm
C
● : contact site
10 µm
D
5 µm
E
Dendrogram (basal dendrites)
: contact site
soma
100
200
300
Distance from soma (µm)

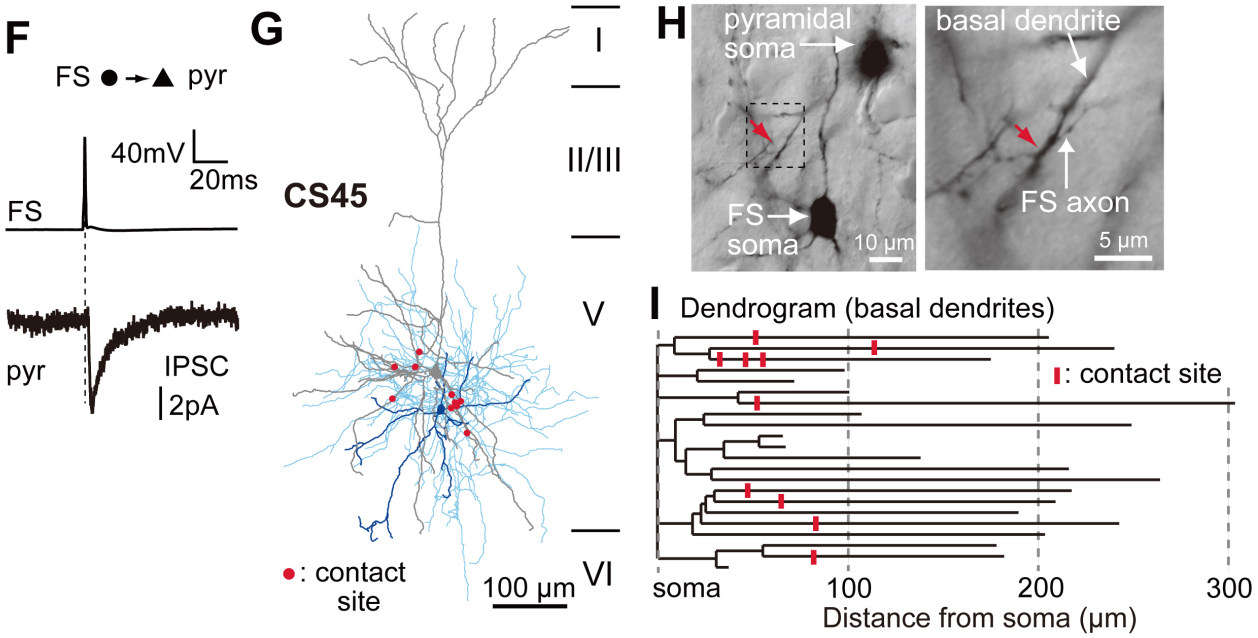
F
FS ● → ▲ pyr
40mV
20ms
FS
pyr
IPSC
2pA
G
CS45
I
II/III
V
VI
● : contact site
100 µm
H
pyramidal soma
FS soma
10 µm
basal dendrite
FS axon
5 µm
I
Dendrogram (basal dendrites)
: contact site
soma
100
200
300
Distance from soma (µm)

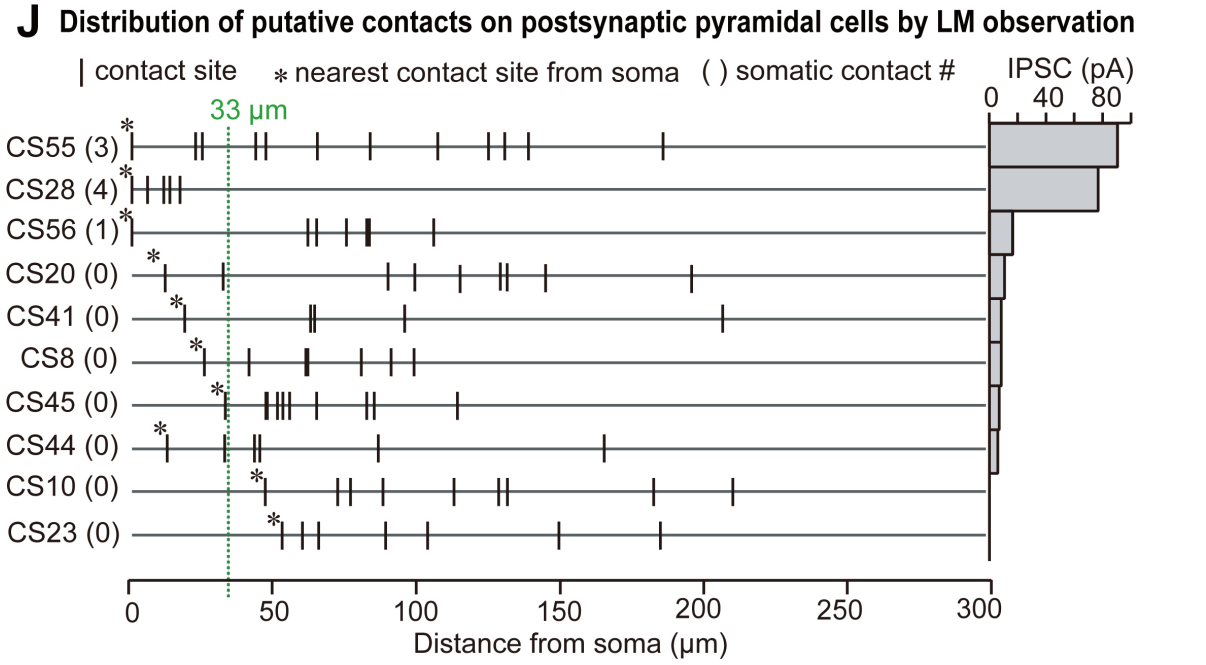
J Distribution of putative contacts on postsynaptic pyramidal cells by LM observation
| contact site
∗ nearest contact site from soma
( ) somatic contact #
IPSC (pA)
0 40 80
33 µm
CS55 (3)
CS28 (4)
CS56 (1)
CS20 (0)
CS41 (0)
CS8 (0)
CS45 (0)
CS44 (0)
CS10 (0)
CS23 (0)
0 50 100 150 200 250 300
Distance from soma (µm)

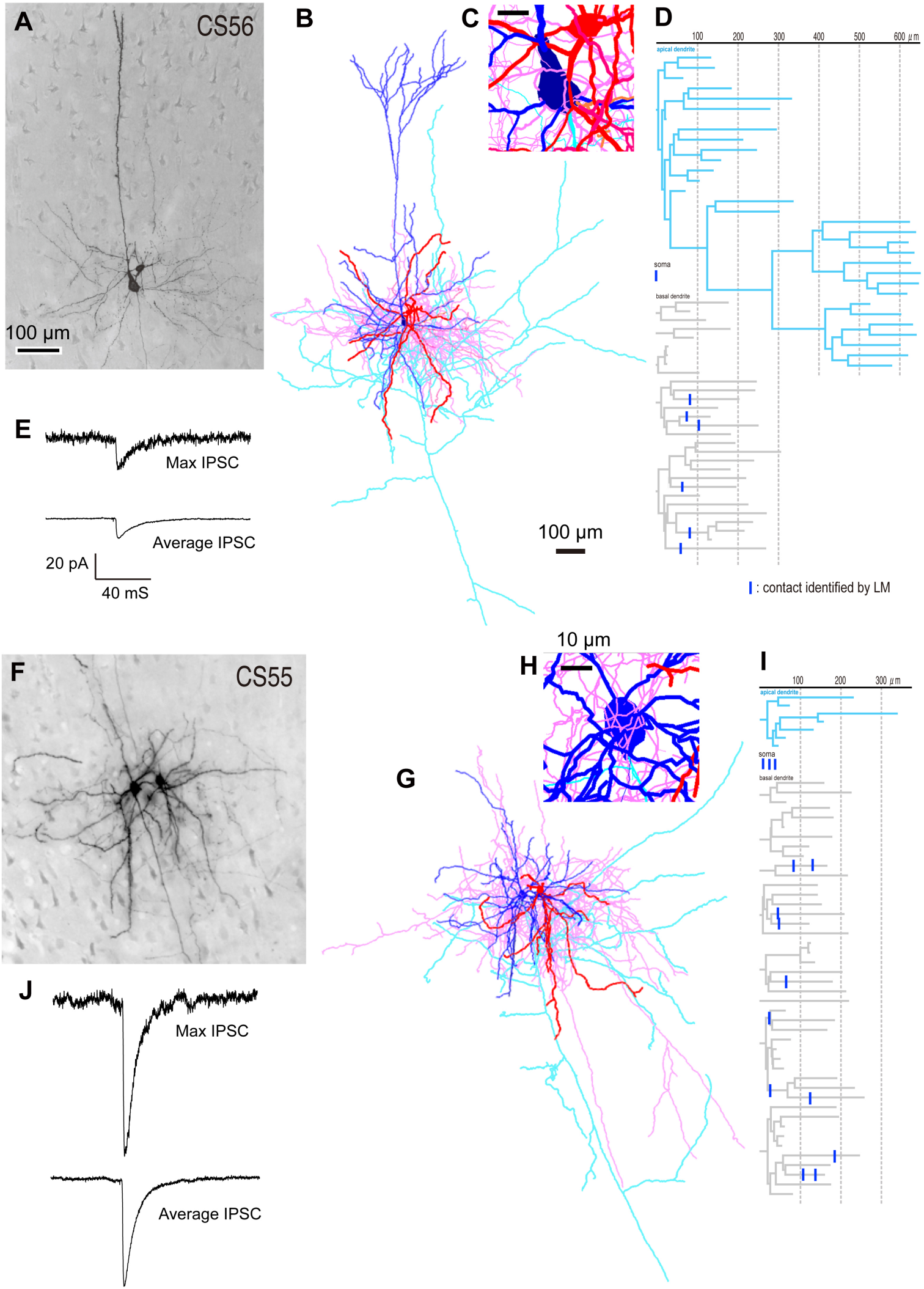
A
CS56
100 µm
B
C
D
100
200
300
400
500
600 µm
apical dendrite
soma
basal dendrite
100 µm
: contact identified by LM
E
Max IPSC
Average IPSC
20 pA
40 mS
F
CS55
10 µm
H
G
I
100
200
300 µm
apical dendrite
soma
basal dendrite
J
Max IPSC
Average IPSC

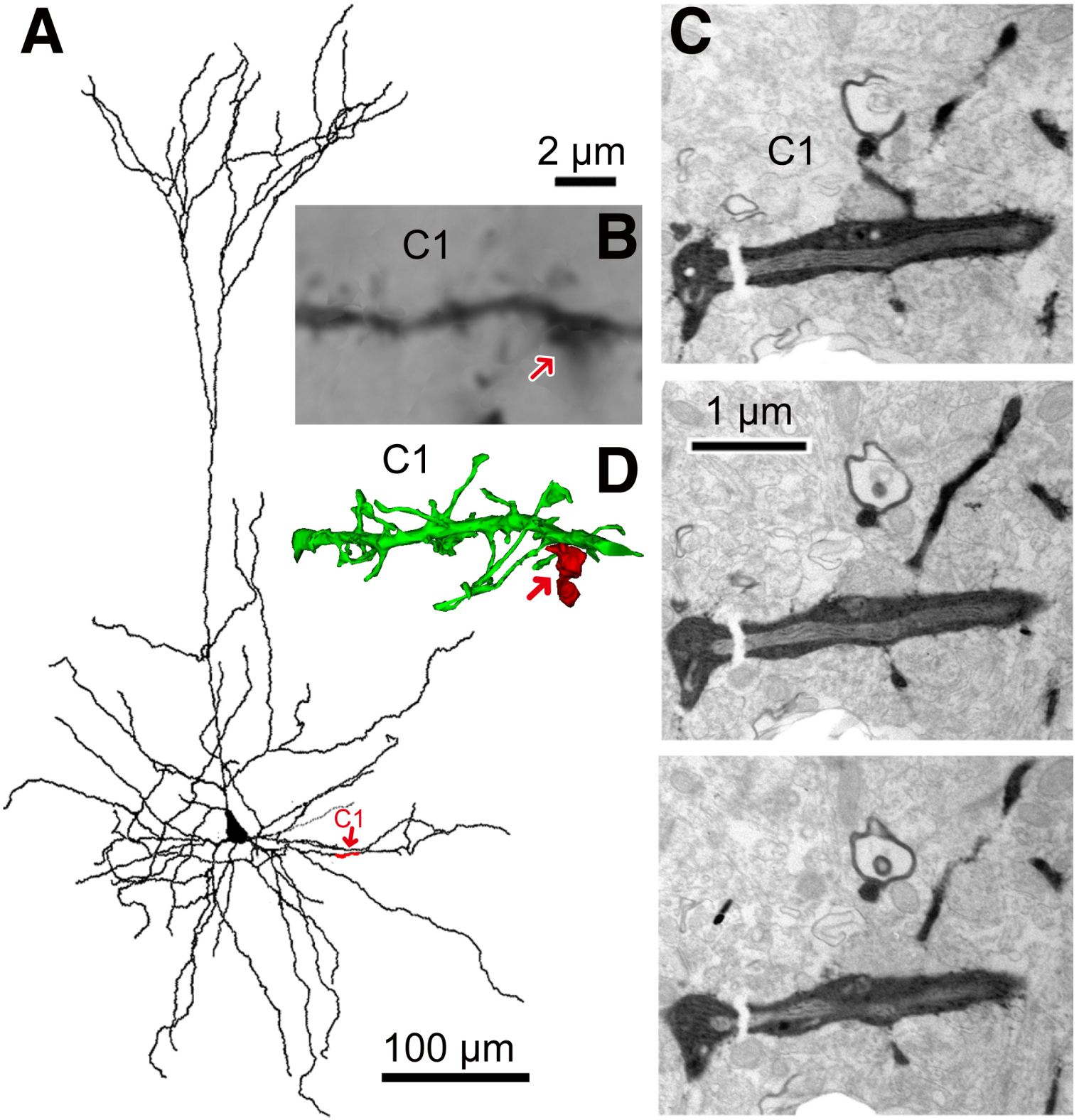
A
2 µm
B
C1
C1
D
C1
100 µm
C
C1
1 µm

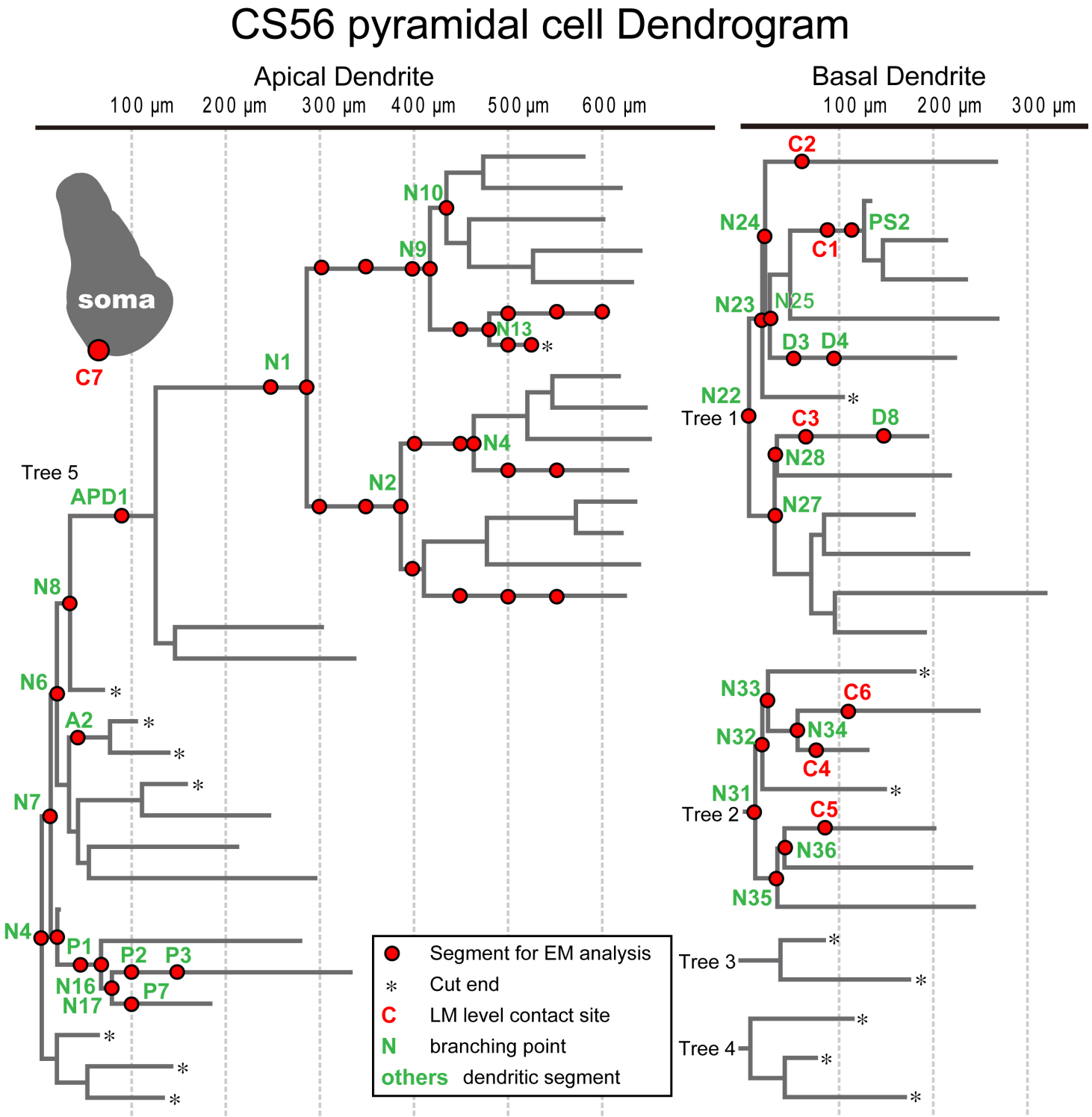
CS56 pyramidal cell Dendrogram
Apical Dendrite
100 µm
200 µm
300 µm
400 µm
500 µm
600 µm
Basal Dendrite
100 µm
200 µm
300 µm
soma
C7
N10
N9
N13
N1
N4
N2
Tree 5
APD1
N8
N6
A2
N7
N4
P1
P2
P3
N16
N17
P7
C2
N24
PS2
C1
N23
N25
D3
D4
N22
Tree 1
C3
D8
N28
N27
N33
C6
N32
N34
C4
N31
Tree 2
C5
N36
N35
Tree 3
Tree 4
Segment for EM analysis
Cut end
C LM level contact site
N branching point
others dendritic segment

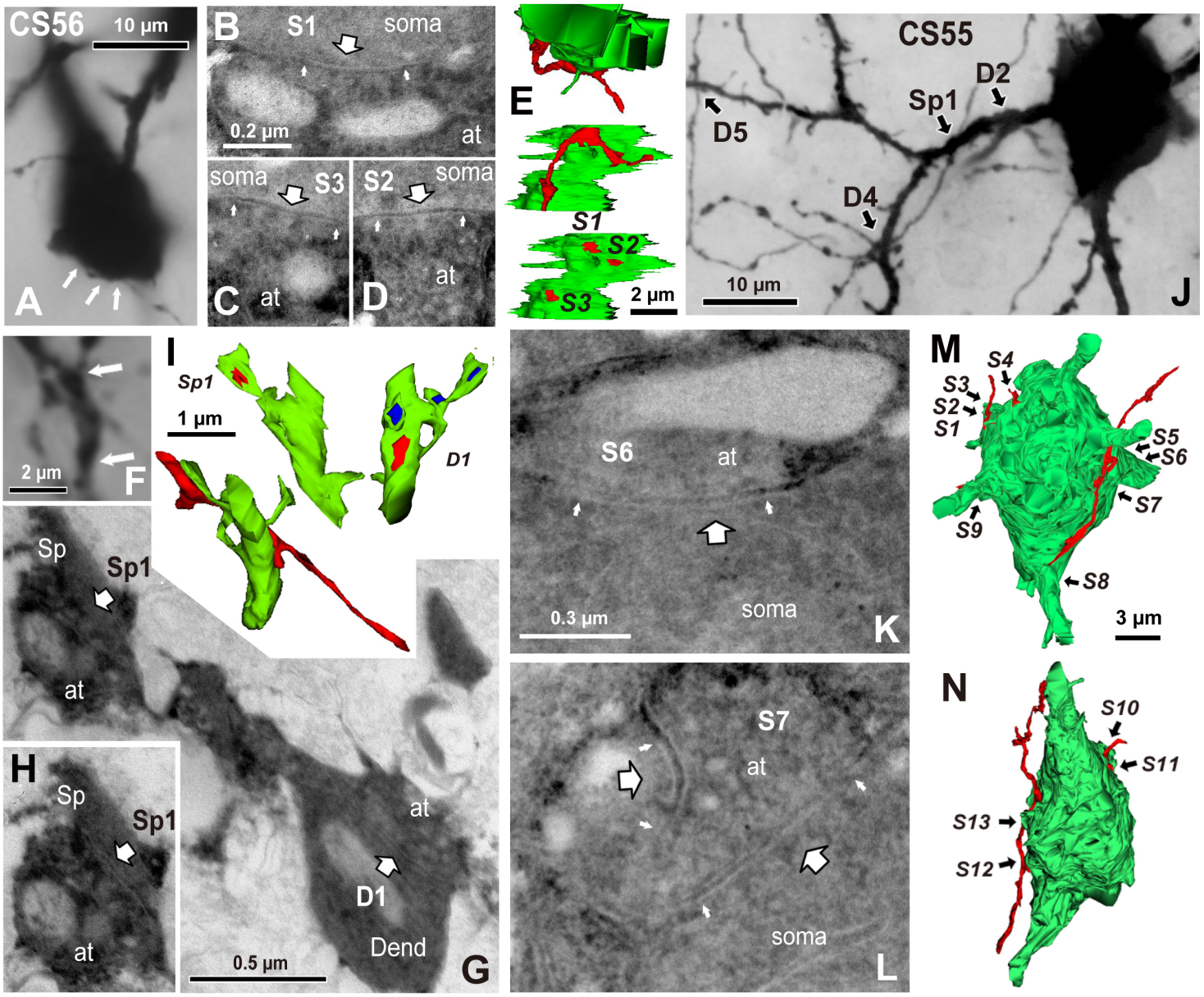
CS56
10 µm
A
B
S1
soma
0.2 µm
at
C
soma
S3
at
D
S2
soma
at
E
S1
S2
S3
2 µm
CS55
D2
Sp1
D5
D4
10 µm
J
F
2 µm
I
Sp1
1 µm
D1
Sp
Sp1
at
H
Sp
Sp1
at
at
D1
Dend
0.5 µm
G
S6
at
0.3 µm
soma
K
M
S4
S3
S2
S1
S5
S6
S7
S9
S8
3 µm
S7
at
soma
L
N
S10
S11
S13
S12

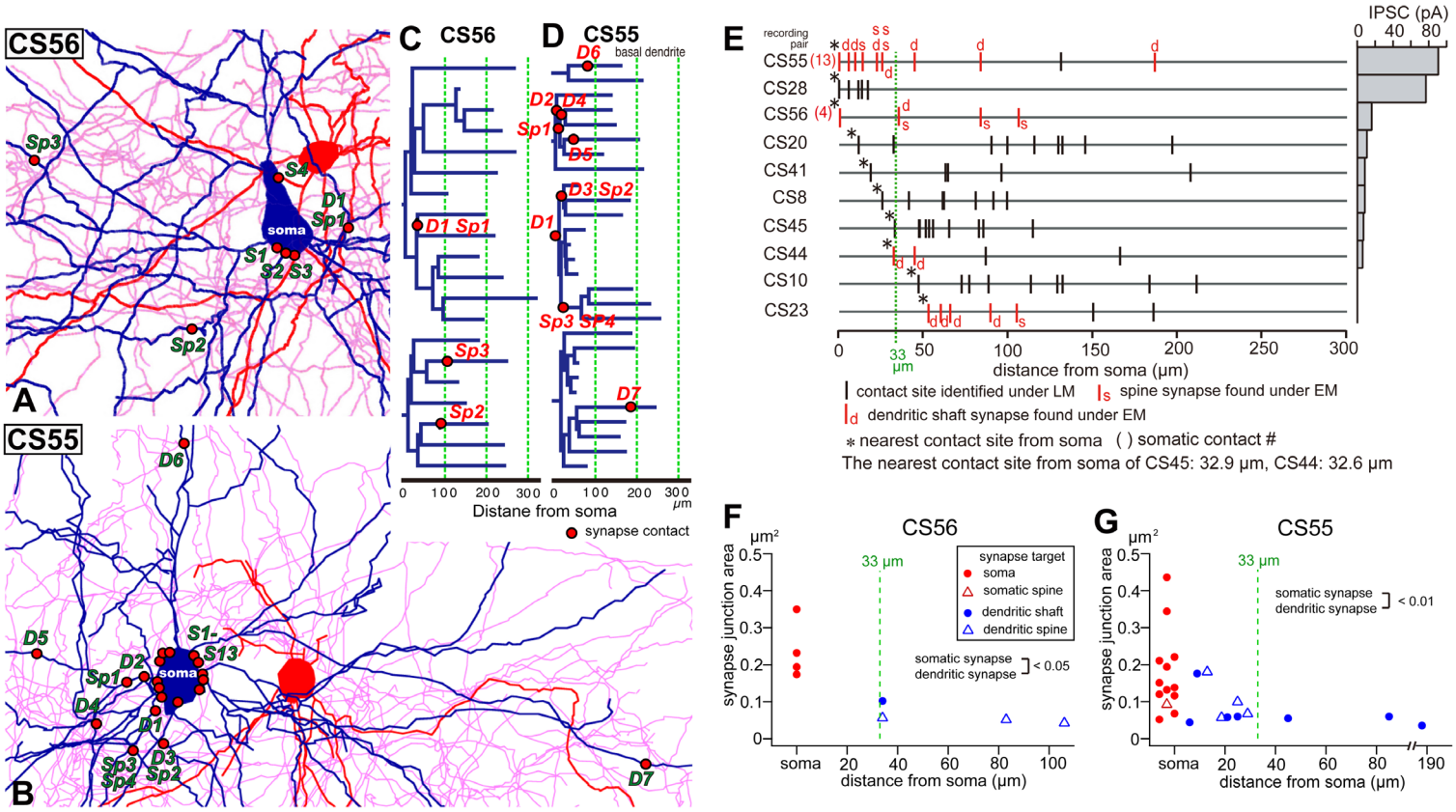
CS56
A
Sp3
S4
D1
Sp1
soma
S1
S2
S3
Sp2
CS55
B
D6
D5
S1-
S13
D2
Sp1
soma
D4
D1
Sp3
Sp4
D3
Sp2
D7
C
CS56
D1 Sp1
Sp3
Sp2
D
CS55
basal dendrite
D6
D2
D4
Sp1
D5
D3 Sp2
D1
Sp3 SP4
D7
0 100 200 300
0 100 200 300 μm
Distane from soma
synapse contact
E
recording pair
IPSC (pA)
0 40 80
CS55 (13)
CS28
CS56 (4)
CS20
CS41
CS8
CS45
CS44
CS10
CS23
0 33 μm 50 100 150 200 250 300
distance from soma (μm)
contact site identified under LM
s spine synapse found under EM
d dendritic shaft synapse found under EM
nearest contact site from soma
( ) somatic contact #
The nearest contact site from soma of CS45: 32.9 μm, CS44: 32.6 μm
F
CS56
μm²
synapse junction area
0 0.1 0.2 0.3 0.4 0.5
33 μm
synapse target
soma
somatic spine
dendritic shaft
dendritic spine
somatic synapse
dendritic synapse
< 0.05
soma 20 40 60 80 100
distance from soma (μm)
G
CS55
μm²
synapse junction area
0 0.1 0.2 0.3 0.4 0.5
33 μm
somatic synapse
dendritic synapse
< 0.01
soma 20 40 60 80 190
distance from soma (μm)

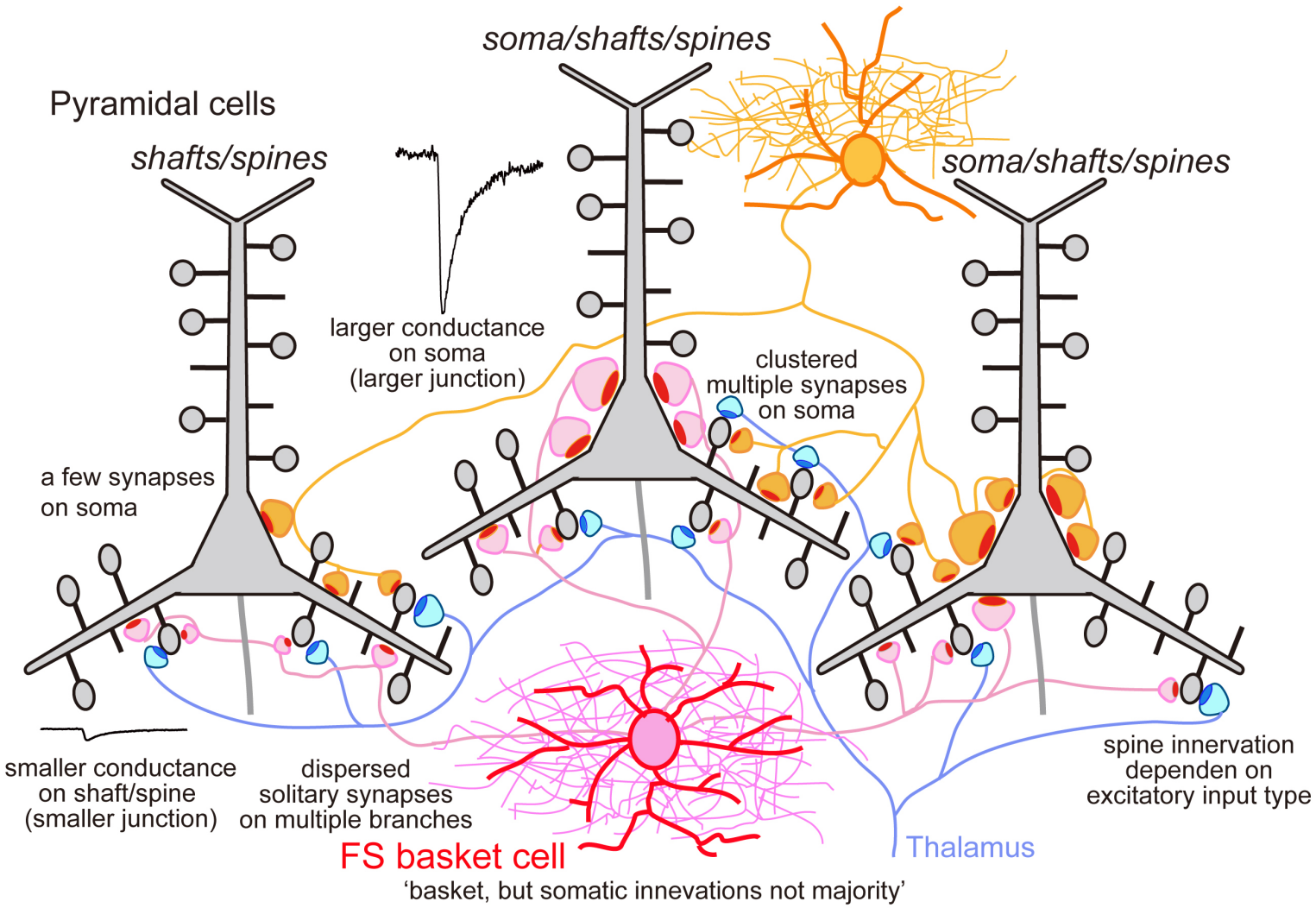
soma/shafts/spines
Pyramidal cells
shafts/spines
soma/shafts/spines
larger conductance
on soma
(larger junction)
clustered
multiple synapses
on soma
a few synapses
on soma
smaller conductance
on shaft/spine
(smaller junction)
dispersed
solitary synapses
on multiple branches
spine innervation
dependen on
excitatory input type
FS basket cell
Thalamus
‘basket, but somatic innevations not majority’

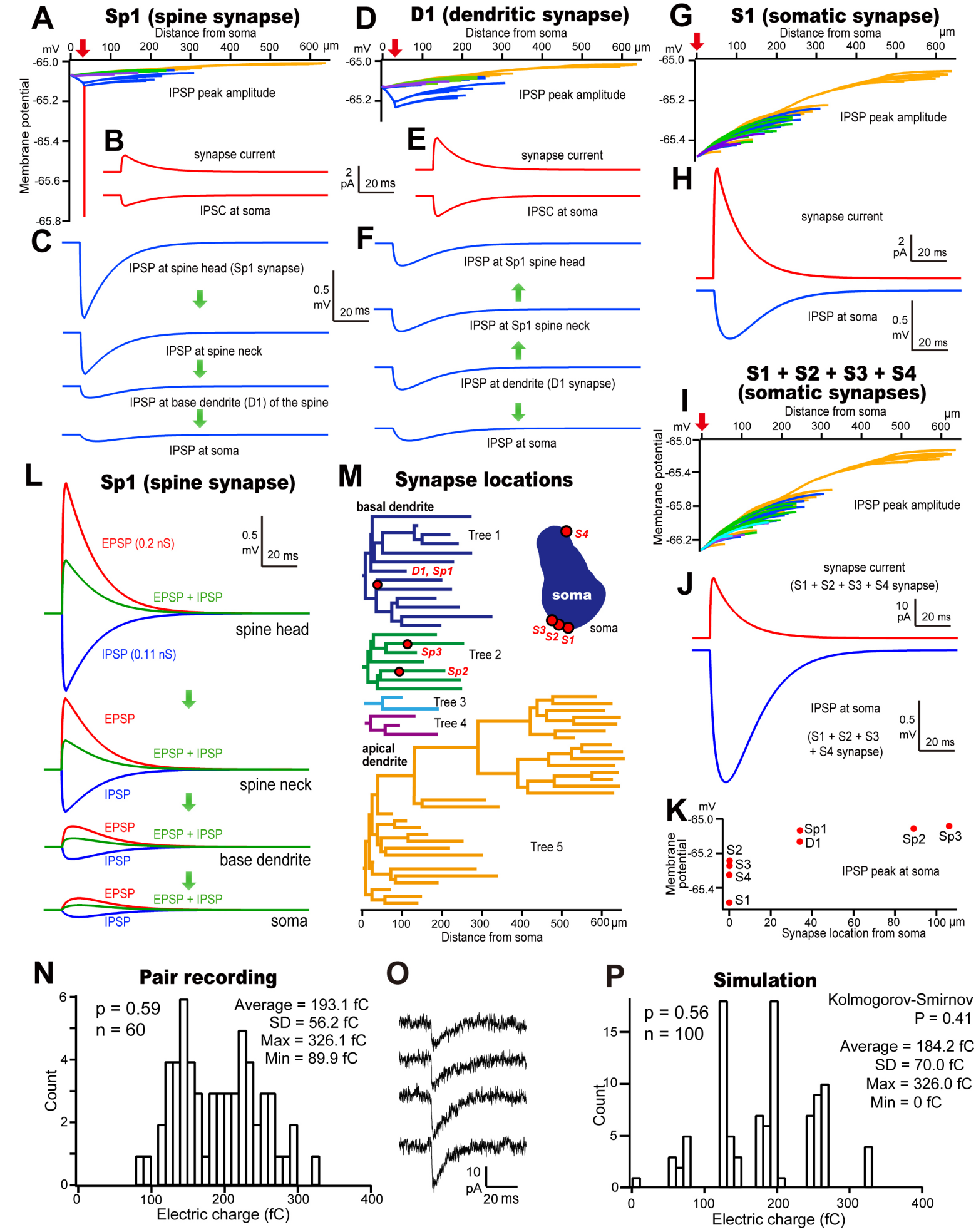
A
Sp1 (spine synapse)
Distance from soma
mV 0 100 200 300 400 500 600 µm
-65.0
-65.2
-65.4
-65.6
-65.8
Membrane potential
IPSP peak amplitude
B
synapse current
IPSC at soma
C
IPSP at spine head (Sp1 synapse)
0.5 mV
20 ms
IPSP at spine neck
IPSP at base dendrite (D1) of the spine
IPSP at soma
D
D1 (dendritic synapse)
Distance from soma
mV 0 100 200 300 400 500 600 µm
-65.0
-65.2
IPSP peak amplitude
E
synapse current
2 pA
20 ms
IPSC at soma
F
IPSP at Sp1 spine head
IPSP at Sp1 spine neck
IPSP at dendrite (D1 synapse)
IPSP at soma
G
S1 (somatic synapse)
Distance from soma
µm
mV 100 200 300 400 500 600
-65.0
-65.2
-65.4
IPSP peak amplitude
H
synapse current
2 pA
20 ms
IPSP at soma
0.5 mV
20 ms
I
S1 + S2 + S3 + S4 (somatic synapses)
Distance from soma
µm
mV 100 200 300 400 500 600
-65.0
-65.4
-65.8
-66.2
Membrane potential
IPSP peak amplitude
J
synapse current
(S1 + S2 + S3 + S4 synapse)
10 pA
20 ms
IPSP at soma
(S1 + S2 + S3 + S4 synapse)
0.5 mV
20 ms
K
mV
-65.0
-65.2
-65.4
Membrane potential
Sp1
D1
Sp2
Sp3
S2
S3
S4
S1
IPSP peak at soma
0 20 40 60 80 100 µm
Synapse location from soma
L
Sp1 (spine synapse)
EPSP (0.2 nS)
0.5 mV
20 ms
EPSP + IPSP
spine head
IPSP (0.11 nS)
EPSP
EPSP + IPSP
spine neck
IPSP
EPSP
EPSP + IPSP
IPSP
base dendrite
EPSP
EPSP + IPSP
IPSP
soma
M
Synapse locations
basal dendrite
Tree 1
D1, Sp1
Tree 2
Sp3
Sp2
Tree 3
Tree 4
apical dendrite
Tree 5
S4
soma
S3 S2 S1
soma
0 100 200 300 400 500 600 µm
Distance from soma
N
Pair recording
p = 0.59
n = 60
Average = 193.1 fC
SD = 56.2 fC
Max = 326.1 fC
Min = 89.9 fC
Count
0 2 4 6
0 100 200 300 400
Electric charge (fC)
O
10 pA
20 ms
P
Simulation
p = 0.56
n = 100
Kolmogorov-Smirnov
P = 0.41
Average = 184.2 fC
SD = 70.0 fC
Max = 326.0 fC
Min = 0 fC
Count
0 5 10 15
0 100 200 300 400
Electric charge (fC)

# Contact sites in dendrogram

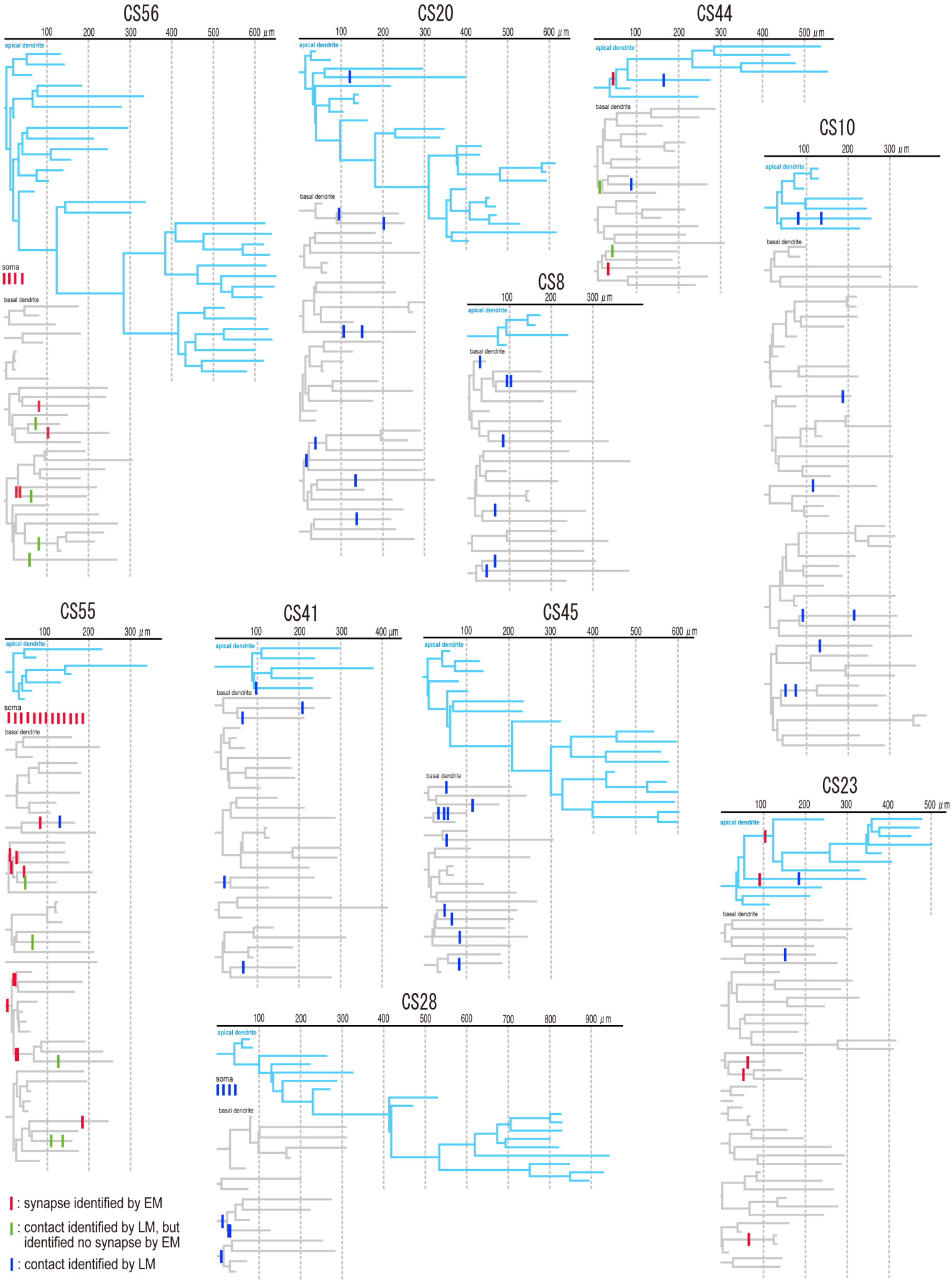

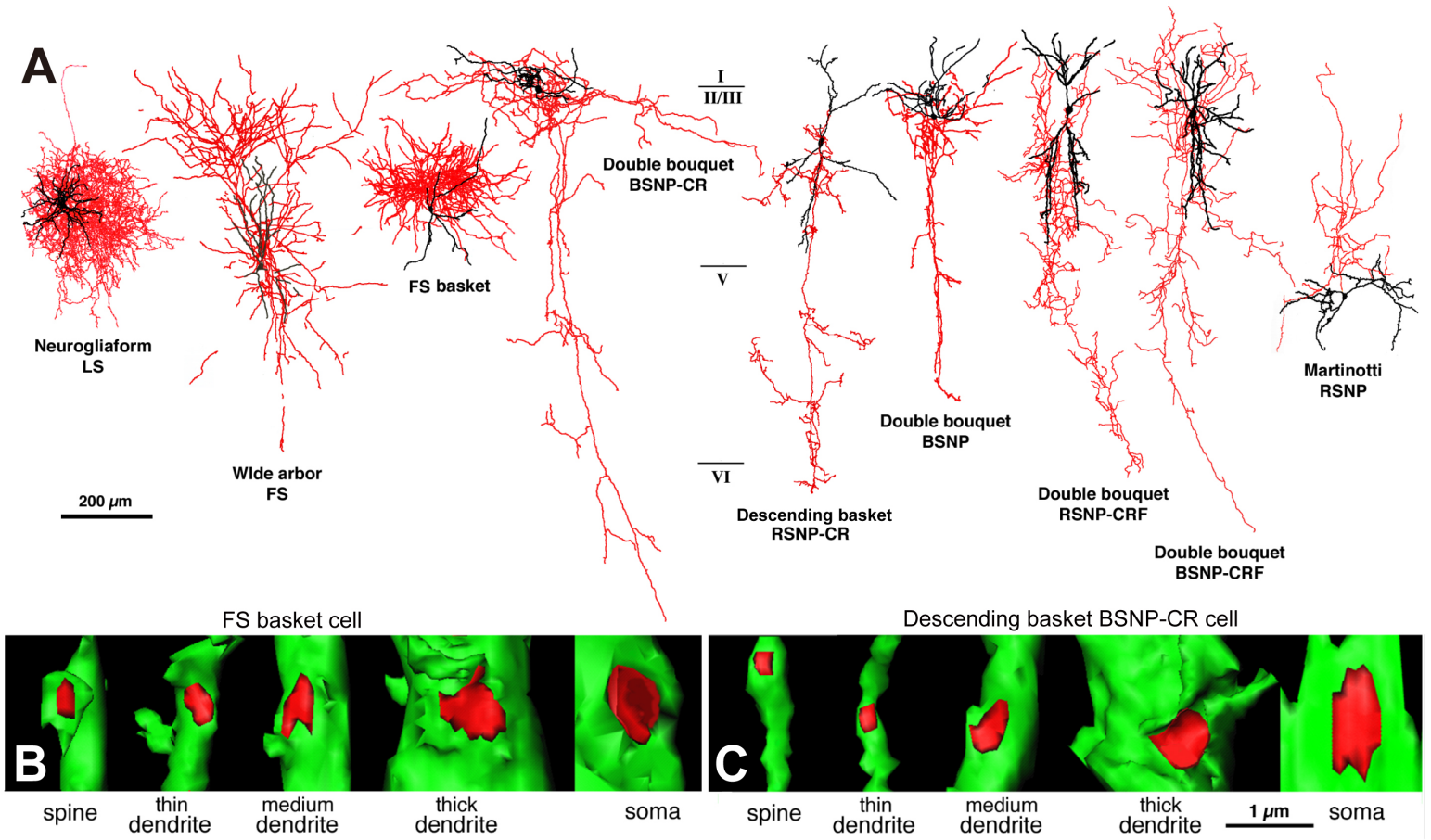
A
I
II/III
V
VI
Neurogliaform LS
FS basket
Wide arbor FS
Double bouquet BSNP-CR
Descending basket RSNP-CR
Double bouquet BSNP
Double bouquet RSNP-CRF
Double bouquet BSNP-CRF
Martinotti RSNP
200 μm


FS basket cell
Descending basket BSNP-CR cell
B
C
spine
thin dendrite
medium dendrite
thick dendrite
soma
1 μm

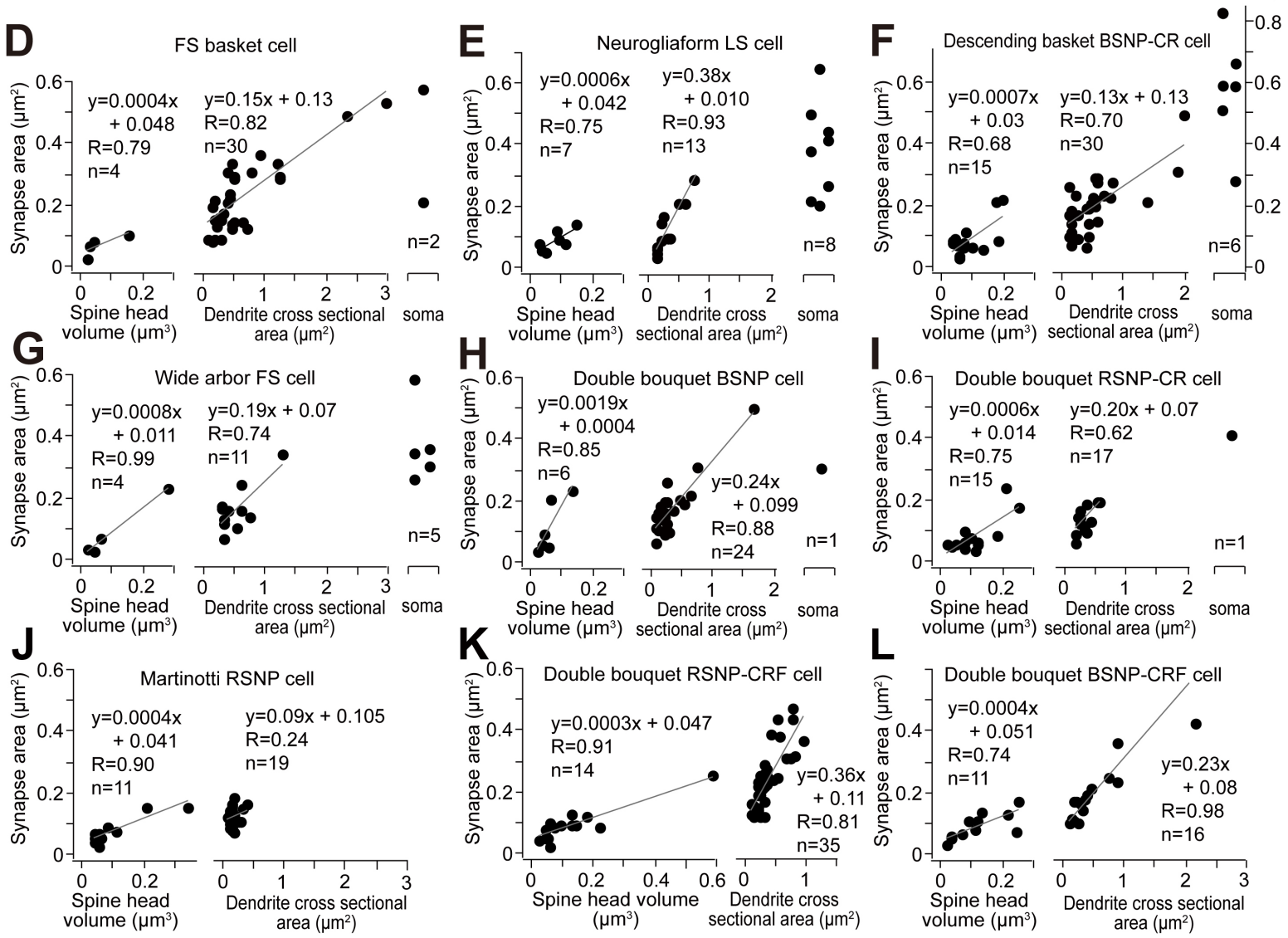
D
FS basket cell
y=0.0004x + 0.048
R=0.79
n=4
y=0.15x + 0.13
R=0.82
n=30
n=2
E
Neurogliaform LS cell
y=0.0006x + 0.042
R=0.75
n=7
y=0.38x + 0.010
R=0.93
n=13
n=8
F
Descending basket BSNP-CR cell
y=0.0007x + 0.03
R=0.68
n=15
y=0.13x + 0.13
R=0.70
n=30
n=6
G
Wide arbor FS cell
y=0.0008x + 0.011
R=0.99
n=4
y=0.19x + 0.07
R=0.74
n=11
n=5
H
Double bouquet BSNP cell
y=0.0019x + 0.0004
R=0.85
n=6
y=0.24x + 0.099
R=0.88
n=24
n=1
I
Double bouquet RSNP-CR cell
y=0.0006x + 0.014
R=0.75
n=15
y=0.20x + 0.07
R=0.62
n=17
n=1
J
Martinotti RSNP cell
y=0.0004x + 0.041
R=0.90
n=11
y=0.09x + 0.105
R=0.24
n=19
K
Double bouquet RSNP-CRF cell
y=0.0003x + 0.047
R=0.91
n=14
y=0.36x + 0.11
R=0.81
n=35
L
Double bouquet BSNP-CRF cell
y=0.0004x + 0.051
R=0.74
n=11
y=0.23x + 0.08
R=0.98
n=16
Synapse area (μm²)
Spine head volume (μm³)
Dendrite cross sectional area (μm²)
soma